Rheology of the Upper Mantle and the Mantle Wedge: A View from the Experimentalists

Greg Hirth

Department of Geology and Geophysics, Woods Hole Oceanographic Institution, Woods Hole, Massachusetts

David Kohlstedt

Department of Geology and Geophysics, University of Minnesota, Minneapolis, Minnesota

In this manuscript we review experimental constraints for the viscosity of the upper mantle. We first analyze experimental data to provide a critical review of flow law parameters for olivine aggregates and single crystals deformed in the diffusion creep and dislocation creep regimes under both wet and dry conditions. Using reasonable values for the physical state of the upper mantle, the viscosities predicted by extrapolation of the experimental flow laws compare well with independent estimates for the viscosity of the oceanic mantle, which is approximately 10^{19} Pa s at a depth of ~100 km. The viscosity of the mantle wedge of subduction zones could be even lower if the flux of water through it can result in olivine water contents greater than those estimated for the oceanic asthenosphere and promote the onset of melting. Calculations of the partitioning of water between hydrous melt and mantle peridotite suggest that the water content of the residue of arc melting is similar to that estimated for the asthenosphere. Thus, transport of water from the slab into the mantle wedge can continually replenish the water content of the upper mantle and facilitate the existence of a low viscosity asthenosphere.

INTRODUCTION

From the alteration of crust at oceanic spreading centers to the migration of melt through the lithosphere at convergent margins, the rheology of rocks plays a key role in the dynamics and chemical fluxes associated with the "Subduction Factory". Consider the following examples: (1) Altered oceanic lithosphere is a source of fluid for hydrous arc magmatism. The amount of water available for melt generation depends on the depth and distribution of hydrothermal alteration of the oceanic lithosphere, which in turn depends on the depth to the brittle-plastic transition. (2) Subducted pelagic sediments also supply fluids to the source of arc magmatism. In this case, the amount of water available depends on the rheology and permeability of the compacting sediments. (3) The kinetics and spatial distribution of dehydration and melting reactions depend on the thermal structure of the slab-mantle interface, which is partly controlled by rheology through the effects of shear heating. (4) The temperature at the slab-mantle interface and in the mantle wedge also depend on the kinematics and dynamics of convection, which in turn are controlled by the viscosity of the mantle wedge. (5) The rheology, fluid

Inside the Subduction Factory
Geophysical Monograph 138
Copyright 2003 by the American Geophysical Union
10.1029/138GM06

distribution and permeability of the slab determine whether fluids migrate into the mantle wedge by porous flow, transport in hydrofractures or advection in diapirs. (6) Finally, melt migration to the base of the crust beneath the arc front and transport of material to back arc spreading centers are governed by mantle flow in the wedge.

It is beyond the scope of this article to address each of these topics in detail. We therefore concentrate on experimental constraints on the viscosity of the mantle wedge. We first review experimental studies used to determine flow law parameters for both dislocation creep and diffusion creep under dry and wet conditions. These data provide insights into the Subduction Factory, as well as other upper mantle tectonic settings, and input for geodynamic models. We then emphasize topics for which progress is needed from experimentalists. Finally, we compare the experimental results with independent geophysical constraints on mantle viscosity.

Viscosity of the Mantle Wedge

The thermal structure of the mantle wedge and the processes that accommodate melt migration to arc volcanoes are in large part controlled by the viscosity of the mantle. Some portions of the mantle wedge may have a lower viscosity than any other region of the upper mantle. Estimates for the viscosity of the oceanic asthenosphere, based on geophysical observations and experimental data on the rheology of peridotite, range from 10^{18} to 10^{19} Pas [e.g., *Melosh,* 1976, *Craig and McKenzie,* 1986; *Hager,* 1991; *Karato and Wu,* 1993; *Hirth and Kohlstedt,* 1996]. There are several reasons why the viscosity of the mantle wedge could be even lower than that in the oceanic asthenosphere. First, the water content in parts of the mantle wedge could be higher than that in the asthenosphere due to the influx of fluids from the subducted slab. Experimental observations indicate that the viscosity of olivine aggregates decreases with increasing water content [e.g., *Mei and Kohlstedt,* 2000b; *Karato,* this issue]. Olivine in the oceanic asthenosphere contains ~1000 H/10^6Si, which is approximately 20% of the solubility at a depth of 120 km [*Hirth and Kohlstedt,* 1996]. At similar depths the mantle wedge may contain as much as 5 times more water (i.e., it may be water saturated). Second, because of the higher water content, drying out of the nominally anhydrous minerals due to partial melting of the wedge will not result in as large of an increase in viscosity as proposed for the melting region of mid-ocean ridges [e.g., *Hirth and Kohlstedt,* 1996; *Phipps Morgan,* 1997]. In fact, depending on the degree of melting, the flux of volatiles from the subducting slab, and the amount of melt retained in the source, partial melting may decrease the viscosity of the wedge. For a constant olivine water content, experimental data indicate that the viscosity of olivine aggregates decreases approximately exponentially with increasing melt content [*Kelemen et al.,* 1997; *Kohlstedt et al.,* 2000; *Mei et al.,* 2002]. Finally, based on the petrological and geophysical data discussed by *Kelemen et al.* [this issue], the temperature in the mantle wedge may be approximately the same as that in the oceanic asthenosphere. Taken together, these observations suggest that in some regions of the mantle wedge the viscosity may be up to an order of magnitude lower than that in the oceanic asthenosphere. In the following sections, we provide a detailed review of the rheological data used to obtain these constraints on mantle viscosity.

Experimental Background

Experimental studies constrain the magnitude of mantle viscosity. However, due to the required extrapolation from laboratory to geologic conditions, the accuracy of these constraints is not as high as their precision. Thus, the laboratory data provide stronger constraints on the change in viscosity as a function of pressure, temperature, grain size, water content and melt fraction. Laboratory experiments are usually conducted near upper mantle temperatures. Therefore, the primary limitation on accuracy comes from the relatively large extrapolation in stress. For example, by extrapolating two orders of magnitude in stress (e.g., from 100 to 1 MPa), an uncertainty in the stress exponent of ± 0.5 results in $\pm$ one order of magnitude uncertainty in viscosity. Another potential problem is that the dominant deformation mechanism may change from dislocation creep to diffusion creep with decreasing stress, provided that grain growth is kinetically inhibited.

While there is uncertainty associated with extrapolation of laboratory results, several observations justify applying experimental flow laws to the study of deformation at geologic conditions. First, a comparison of microstructures in experimentally and naturally deformed peridotites indicates that the same slip systems are active [e.g., *Nicolas,* 1986]. The analysis of lattice preferred orientations in both naturally and experimentally deformed rocks demonstrates that strain is mostly accommodated by slip on (010)[100] [e.g., *Tomassi et al.,* 1999; *Zhang et al.,* 2000], the easiest slip system in olivine [e.g., *Durham and Goetze,* 1977; *Bai et al.,* 1991]. Second, the conditions under which changes in deformation mechanism occur can be constrained using a combination of experimental data and theoretical arguments. For example, diffusion creep processes can be studied using experimentally engineered fine-grained aggre-

gates. Viscosity in the diffusion creep regime increases non-linearly with increasing grain size. Thus, rocks with a grain size of 10 μm (which is two to three orders of magnitude smaller than the grain size in most of the mantle) will deform six to nine orders of magnitude faster by diffusion creep in the laboratory than larger grained rocks in the mantle. Likewise, because viscosity in the dislocation creep regime decreases non-linearly with increasing stress, experiments can be carried out to high strain in both deformation regimes at laboratory timescales.

The strategy of using fine-grained aggregates synthesized from natural rocks and minerals has lead to several breakthroughs in our understanding of the rheology of peridotite. The primary benefit of these types of experiments is that a large number of extensive parameters can be controlled independently, including melt fraction, grain size and water content. In addition, sample-to-sample variability is significantly decreased by the application of standard protocols for sample preparation. Many of the flow law parameters in which we have the highest confidence are determined this way. However, one drawback of this procedure is that many experiments are conducted near the transition between diffusion and dislocation creep. To obtain the highest resolution in flow law parameters for individual creep mechanisms, the component of strain rate from competing deformation processes to the total strain rate must be taken into account. This problem is outlined below in our review of flow law parameters for diffusion and dislocation creep.

CONSTRAINTS ON FLOW LAW PARAMETERS

Theoretical treatments and experimental observations demonstrate that the rheological behavior of rocks, metals and ceramics is well described by a power law dependence of strain rate ($\dot{\varepsilon}$) on differential stress (σ). For olivine aggregates, we use a power law of the form

$$\dot{\varepsilon} = A\sigma^n d^{-p} fH_2O^r \exp(\alpha\phi)\exp\left(-\frac{E^*+PV^*}{RT}\right) \quad (1)$$

where A is a constant, n is the stress exponent, d is grain size, p is the grain size exponent, fH_2O is water fugacity, r is the water fugacity exponent, ϕ is melt fraction, α is a constant, E^* is the activation energy, V^* is the activation volume, R is the gas constant, and T is absolute temperature. In the sections below, we review experimental constraints for these flow law parameters for deformation in the diffusion creep and dislocation creep regimes, as well as provide some constraints on flow law parameters for deformation accommodated by grain boundary sliding. We first review the stress dependence of deformation, followed by analyses of the influence of temperature, pressure, water content, and melt fraction. We do not review the flow law parameters for individual deformation mechanisms seperately because our analysis includes resolving the components of strain rate from competing deformation processes. For those readers wishing to skip the details of how these parameters are constrained, the values of the flow law parameters are summarized in Table 1.

In addition to the parameters in equation (1), the rheology of olivine aggregates also depends on oxygen fugacity (fO_2^q) and silica activity. However, for practical application of flow laws to geodynamic modeling, we have incorporated the influence of oxygen fugacity into A and E^*. Experimental observations indicate that $\dot{\varepsilon} \propto fO_2^q$, where the exponent q is $\leq 1/6$ for a wide range of deformation conditions [*Ricoult and Kohlstedt,* 1985; *Bai et al.,* 1991]. Thus, because the range of oxygen fugacities expected in the mantle is small, the effect of changes in oxygen fugacity on viscosity is relatively minor compared to changes in creep rate that occur due to variations in temperature, water content or pressure. Also, since olivine and pyroxene are both present in most mantle rocks, the silica activity is fixed through out most of the mantle.

Stress Dependence and Grain Size Dependence in the Diffusion Creep Regime

The flow law for diffusion creep under dry conditions is well constrained by experiments conducted on fine-grained rocks [*Karato et al.,* 1986; *Hirth and Kohlstedt,* 1995a, *Gribb and Cooper,* 2000]. These studies built on the pioneering uniaxial hot-pressing experiments of *Schwenn and Goetze* [1978] and *Cooper and Kohlstedt* [1984]. Under dry conditions, the stress exponent ($n = 1.0 \pm 0.1$) and grain size exponent ($p = 3.0 \pm 0.5$) reported by *Hirth and Kohlstedt* [1995a] are in agreement with theoretical predictions for creep dominated by grain boundary diffusion [e.g., *Coble,* 1963]. Several other studies have also yielded values for n and p which are within error of those predicted by the Coble creep equation [e.g., *Cooper and Kohlstedt,* 1984]. As discussed by *Hirth and Kohlstedt* [1995a], the slightly lower value of p and higher value of n reported by Karato et al. [1986] likely reflect a component of dislocation creep to the overall strain rate of the samples. Values of $n \approx 1$ and $p \approx 3$ are also observed under water saturated conditions [*Karato et al.,* 1986; *Mei et al.,* 2000a]. Based on the agreement between these data and the theoretical predictions, we use values of $n = 1$ and $p = 3$ in evaluation of deformation data obtained under conditions for which more than one creep mechanism contributed significantly to flow.

Table 1: Rheological Parameters for Equation (1).

	A^a	n	p	r^b	α	E^* (kJ/mol)	V^* (10^{-6} m^3/mol)
dry diffusion	1.5×10^9	1	3	-	30	375 ± 50	2-10
wet diffusion	$2.5\times10^{7\,d}$	1	3	0.7–1.0	30	375 ± 75	0-20
wet diffusion (constant C_{OH})[c]	1.0×10^6	1	3	1	30	335 ± 75	4
dry dislocation	1.1×10^5	3.5 ± 0.3	0	-	30-45	530 ± 4	(see Table 2)
wet dislocation	1600	3.5 ± 0.3	0	1.2 ± 0.4	30-45	520 ± 40	22 ± 11
wet dislocation (constant C_{OH})[e]	90	3.5 ± 0.3	0	1.2	30-45	480 ± 40	11
dry GBS, T>1250°C	4.7×10^{10}	3.5	2	-	30-45	600[f]	(see Table 2)[g]
dry GBS, T<1250°C	6500	3.5	2	-	30-45	400[f]	(see Table 2)[g]

[a]For stress in MPa, f_{H_2O} in MPa (or C_{OH} in H/10^6Si) and grain size in μm.
[b]Uncertainty in r is correlated with uncertainty in V^*
[c]Example calculation for C_{OH} = 1000 H/10^6Si, d = 10 mm, T = 1400°C, P = 1 GPa, σ = 0.3 MPa:
$\dot{\varepsilon} = (1.0\times10^6)^*(0.3)^1*(10{,}000)^{-3}*(1000)^1*\exp[-(335000+10^9*4\times10^{-6})/(8.314*1673)] = 7.8\times10^{-15}$/s
[d]Value for A is given for r = 1.
[e]Example calculation for C_{OH} = 1000 H/10^6Si, T = 1400°C, P = 1 GPa, σ = 0.3 MPa:
$\dot{\varepsilon} = (90)^*(0.3)^{3.5}*(1000)^{1.2}*\exp[-(480000+10^9*11\times10^{-6})/(8.314*1673)] = 2.5\times10^{-12}$/s
[f]The activation energy for GBS is assumed to be that for slip on (010)[100], which changes with increasing temperature [*Bai et al.*, 1991]. The values given here include the effect of temperature on oxygen fugacity.
[g]The value for V^* is assumed to be the same as that for dislocation creep.

Diffusion creep data can be used to estimate the grain boundary diffusivity of the slowest diffusing species in olivine. Diffusion creep is limited by the slowest diffusing species moving along its fastest path. Therefore, creep rate is governed by an effective diffusivity, $D_{eff} \approx [D_{gm} + \tau\delta D_{gb}/d]$, where D_{gm} is the grain matrix diffusivity, D_{gb} is the grain boundary diffusivity, δ is the grain boundary width, d is the grain size, and τ is a "tortuosity" constant; we use a value of τ = 1.5. In Figure 1, we compare the rates of grain matrix diffusion under dry conditions of Mg (D^{Mg}_{gm}) [*Gaetani and Watson,* 2000] and Si (D^{Si}_{gm}) [*Houlier et al.,* 1990] to rates for bulk grain boundary diffusion of Mg (D^{Mg}_{bulk}) [from *Watson,* 1991 (see *Hirth and Kohlstedt,* 1995a)] and Si (D^{Si}_{bulk}) [*Farver and Yund,* 2000] at a temperature of 1300°C, where $D_{bulk} = \tau\delta D_{gb}/d$. In addition, we plot the effective diffusivity determined from the rate of diffusion creep. In this case, we plot $\tau\delta D_{gb}/d$, where the product δD_{gb} is calculated from observed creep rates using the theoretical Coble creep flow law [e.g., *Karato et al.,* 1986; *Hirth and Kohlstedt,* 1995a]. These relationships indicate that diffusion creep is limited by grain boundary diffusion of silicon [e.g., *Hirth and Kohlstedt,* 1995a, *Farver and Yund,* 2000]. Based on the observation that both the grain boundary and grain matrix diffusivities for oxygen lie between the respective values for Mg and Si [e.g., *Fisler and Mackwell,* 1994; *Ryerson et al.,* 1989], we have omitted them from this figure. The diffusion data for Mg are included to check whether conditions exist where $D^{Si}_{bulk} > D^{Mg}_{gm}$, as suggested by *Karato et al.* [1986]. A transition to diffusion creep limited by grain matrix diffusion (i.e., Nabarro-Herring creep) is not predicted unless that grain size is greater than approximately 1m. This calculation, which demonstrates that Nabarro-Herring creep is unlikely to

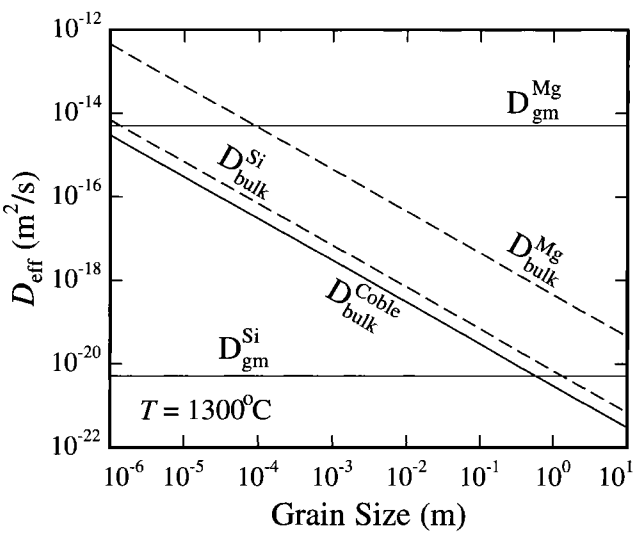

Figure 1. Plot of effective diffusivity at 1300°C versus grain size, comparing bulk diffusivities of silicon and magnesium via grain boundary transport to grain matrix (gm) diffusivities. The bulk diffusivity calculated using diffusion creep deformation data for olivine aggregates is also shown (D^{Coble}_{bulk}). These relationships indicate that diffusion creep is limited by D^{Si}_{bulk} unless the grain size is greater than ~1 m.

occur in experiments or at any conditions in the upper mantle, further justifies using $p = 3$ to normalize diffusion creep data to a common grain size. A similar analysis can not be carried out for hydrous conditions because of a lack of diffusion data.

Stress Dependence in the Dislocation Creep Regime: Dry Conditions

Much of the highest resolution mechanical data, such as that shown in Figure 2a, are acquired on fine-grained olivine aggregates deformed at the transition between diffusion creep and dislocation creep. To determine the stress exponent in the dislocation creep regime, we have accounted for the diffusion creep component of the data in two ways. In the first approach, we use a non-linear least squares fit of the data at constant temperature and pressure to the equation

$$\dot{\varepsilon} = \dot{\varepsilon}_{\text{disl}} + \dot{\varepsilon}_{\text{diff}} = A_{disl}\sigma^n + A_{diff}\sigma d^{-3} \qquad (2)$$

For the experimental results presented in Figure 2a, the non-linear fit gives $n = 3.3 \pm 0.6$. In the second approach, we subtract the strain rate of the corresponding diffusion creep flow law from the total strain rate, which leaves only the dislocation creep component, and linearly fit only the highest stress data. In this case, we obtain a value of $n = 3.6 \pm 0.5$.

These values for n are comparable to those determined for coarser grained natural rocks deformed at the same conditions [e.g., *Chopra and Paterson,* 1984]. From a global inversion of their data to determine n, E^*, and A, *Chopra and Paterson* obtained $n = 3.6 \pm 0.2$. Their analysis included some data at differential stresses significantly greater than the confining pressure and, therefore, may be influenced by a change in deformation mechanism to semi-brittle flow [e.g., *Evans et al.,* 1990] or "power law breakdown" [e.g., p. 81 *Poirier,* 1985]. By refitting their data excluding all points at differential stresses greater than 300 MPa (i.e., the confining pressure), we obtain $n = 3.4 \pm 0.2$ (using $E^* = 530$ kJ/mol to normalize data to a constant temperature). By fitting only data at a constant temperature of 1573 K and stresses below 300 MPa (this sample is the largest satisfying these criteria, with only 4 data points), we obtain $n = 3.7 \pm 0.4$.

The values of n determined for the polycrystalline samples agree well with those determined for olivine single crystals [e.g., *Kohlstedt and Goetze,* 1974; *Durham and Goetze,* 1977; *Bai et al.,* 1991]. Values of n for the three major slip systems in olivine have been determined over a large range in temperature and oxygen fugacity. Under all of these conditions, n is observed to be in the range of 3.5. Because single crystal experiments can be conducted at 1 atm, the data have high precision at low strain rates and relatively high temperatures. Values of n of ~3.5 are observed at stresses as low as 15 MPa [*Bai et al.,* 1991, *Jin et al.,* 1994]. These data are extremely valuable as they

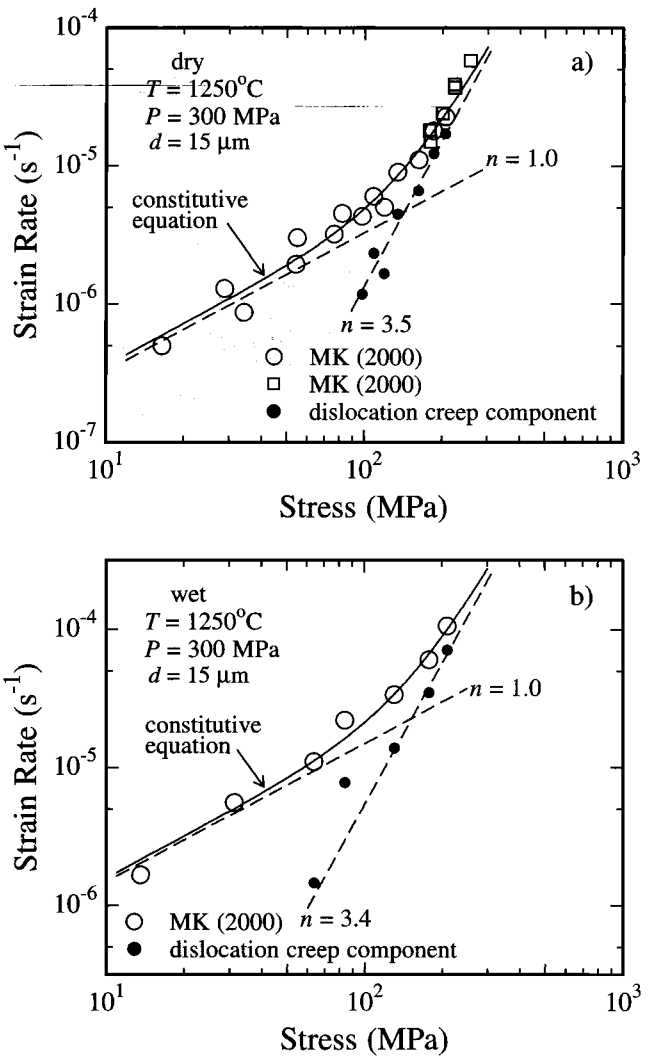

Figure 2. Plots of strain rate versus differential stress for fine-grained olivine aggregates deformed under dry (a) and wet (b) conditions. For both data sets, a transition from diffusion creep to dislocation creep occurs with an increase in differential stress. Non-linear fits to the data using equation 2 (labeled constitutive equation) and linear fits to the high stress dislocation creep component of the total strain rate are shown in both figures. These data are from the studies of *Mei and Kohlstedt* [2000a, 2000b].

significantly decrease the uncertainty in extrapolation to the lower stresses appropriate for the asthenosphere.

Stress Dependence in Dislocation Creep Regime: Wet Conditions

The stress dependence of dislocation creep in the presence of water is also well constrained by a combination of experiments on single crystals, coarse-grained natural dunites, and fine-grained aggregates synthesized from natural crystals. A data set illustrating the transition from diffusion creep to dislocation creep is shown in Figure 2b for an experiment conducted under water-saturated conditions at a confining pressure of 300 MPa. The non-linear least squares fit of the data using equation (2) gives $n = 3.4 \pm 0.5$. A linear fit of the dislocation creep component gives $n = 3.6 \pm 0.6$. The average value of n determined in this manner from the experiments of *Mei and Kohlstedt* [2000b] (7 experiments) is 3.8 ± 0.6. We re-analyzed similar data from the study of *Karato et al.* [1986] and determined $n = 3.6 \pm 0.3$ for the non-linear fit and $n = 3.5 \pm 0.3$ for the linear fit to the dislocation creep component derived by subtracting the diffusion creep component from the total strain rate. *Karato et al.* [1986] report a value of n in the range 3-3.5. Again, these values are similar to those determined for coarse-grained natural dunites and single crystals. As reported in *Hirth and Kohlstedt* [1996], a least squares linear fit to *Chopra and Paterson's* [1981] wet dunite data at a temperature of 1473 K and stresses less than 300 MPa gives $n = 3.4 \pm 0.3$. Similarly, experiments on olivine single crystals deformed under hydrous conditions yields $n = 3.0 \pm 0.1$ to 3.8 ± 0.2 [*Mackwell et al.,* 1985; *Mackwell et al.,* 1997].

In summary, while lower values for the stress exponent have been reported for olivine aggregates under wet conditions [e.g., *Mei and Kohlstedt,* 2000b; *Karato et al.,* 1986; *Karato and Jung,* in press], an analysis of these same data that takes into account the component of diffusion creep to the total strain rate indicates that the stress exponent for dislocation creep is 3.5 ± 0.3 for both wet and dry conditions.

Activation Energy for Diffusion Creep: Dry Conditions

The activation energy for creep and the pre-exponential constant are determined by normalizing diffusion creep data to constant values of stress and grain size using $n = 1$ and $p = 3$. The temperature dependence of diffusion creep determined from several suites of compression experiments is illustrated in Figure 3a. The contribution of dislocation creep has been removed from these data using the fitting procedure described above. The magnitude of the strain rates observed in these four studies agree well. However, relatively few experiments were specifically designed to determine the activation energy for diffusion creep. Indeed, for two of these studies all experiments were conducted at one temperature. Activation energies determined from two experiments on fine-grained dunite range from 310 ± 40 kJ/mol to 440 ± 80 kJ/mol [*Hirth and Kohlstedt,* 1995a]. These values are similar to the value of 430 ± 70 kJ/mol determined by a linear fit to all of the dunite data shown in Figure 3a. Figure 3a also includes data for fine-grained lherzolite samples [*Kohlstedt and Zimmerman,* 1996], which indicate that pyroxene has little effect on deformation in the diffusion creep regime. This observation suggests that diffusion rates along olivine-olivine, pyroxene-pyroxene, and olivine-pyroxene interfaces are similar. If the lherzolite data are included in the fit, the activation energy is lowered to 320 ± 30 kJ/mol.

The activation energy for diffusion creep under dry conditions has also been determined from compression experiments [*Kohlstedt et al.,* 2000], densification experiments [*Schwenn and Goetze,* 1978; *Cooper and Kohlstedt,* 1984], and low strain tortional creep experiments [*Gribb and Cooper,* 1998, 2000] conducted at room pressure. Activation energies determined from densification experiments of $E^* = 380 \pm 105$ kJ/mol [*Cooper and Kohlstedt,* 1984] and $E^* = 360 \pm 120$ kJ/mol [*Schwenn and Goetze,* 1978] agree well with those determined from the high-pressure compression experiments shown in Figure 3a. By contrast, the activation energy determined from the low-pressure compression experiments ($E^* = 530$ kJ/mol, no uncertainty given [*Kohlstedt et al.,* 2000]) is significantly greater. This value may be influenced by cavitation during creep. Likewise, the activation energy determined from the torsion tests of $E^* = 700 \pm 30$ kJ/mol, *Gribb and Cooper* [1998, 2000] is significantly higher. *Gribb and Cooper* [2000] suggest that the higher values for the activation energy result from grain boundary segregation of incompatible components. Based on the agreement between the high-pressure creep tests and the densification tests we conclude that the activation energy is 375 ± 50 kJ/mol.

Activation Energy for Diffusion Creep: Wet Conditions

Few experiments have been conducted to constrain the activation energy for diffusion creep under wet conditions. *Mei and Kohlstedt* [2000a] conducted the only experiments specifically designed to determine the activation energy. Least squares fits to data from two experiments illustrated in Figure 3b show remarkable agreement with $E^* = 380 \pm 20$ kJ/mol and 410 ± 40 kJ/mol. In Figure 3b, the dislocation creep component for each individual experiment is subtracted from the total strain rate using the fitting

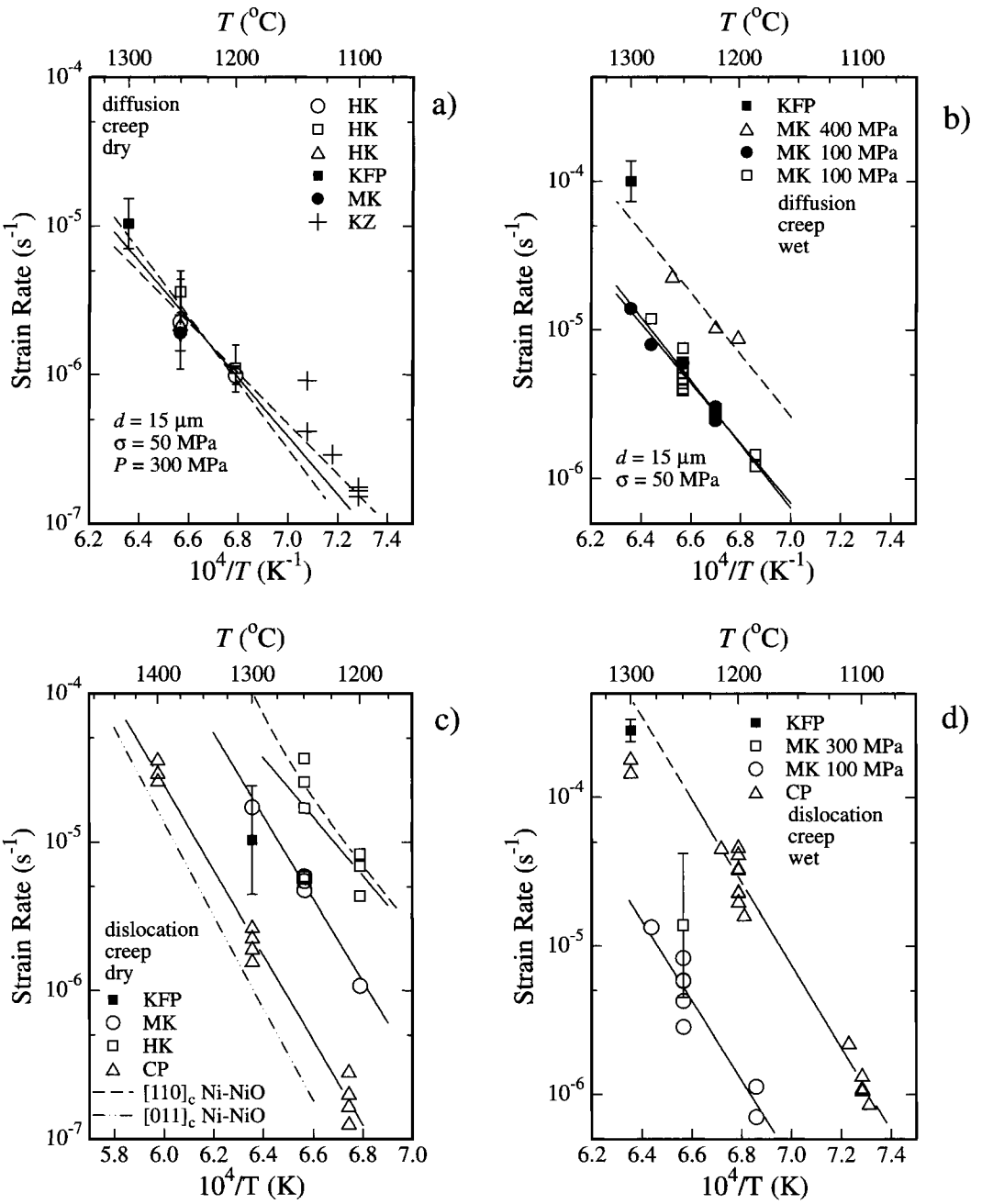

Figure 3. Arrhenius plots of strain rate versus 1/T for olivine aggregates deformed in the diffusion creep regime (a and b) and dislocation creep regime (c and d) under both dry and wet conditions. (a) Dry diffusion creep data: The solid line and dashed lines show the Arrhenius relationships for E^* = 375±50 kJ/mol. (b) Wet diffusion creep data: Least squares fits shown for the two 100 MPa data sets give E^* = 380 ± 20 kJ/mol and 410 ± 40 kJ/mol, respectively. (c) Dry dislocation creep data: Least squares fits to the data of *Chopra and Paterson* [1984] (CP) and *Mei and Kohlstedt* [2000] (MK) give E^* = 530 ± 40 and E^* = 550 ± 20 kJ/mol, respectively. Strain rates for olivine single crystals [*Bai et al.,* 1991] are also shown. (d) Wet dislocation creep data: A least squares fit to the 100 MPa data of *Mei and Kohlstedt* (MK) gives E^* = 510 ± 70 kJ/mol, which is in good agreement with the value of 530 ± 30 kJ/mol determined for the data of Chopra and Paterson (CP). HK = *Hirth and Kohlstedt* [1995a,b]; KFP = *Karato et al.* [1986]; MK = *Mei and Kohlstedt* [2000a,b]; KZ = *Kohlstedt and Zimmerman* [1996].

procedure detailed above. By accounting for the component of dislocation creep in these data, the activation energy appears to be greater than the published value of 300 kJ/mol [*Mei and Kohlstedt,* 2000a]. These values are not significantly influenced by uncertainty in n and E^* in the dislocation creep regime. For example, by allowing E^*_{disl} to vary from 450 to 550 kJ/mol and n_{disl} to vary from 3 to 4, the values of E^*_{diff} vary from 350 ± 30 to 440 ± 40 kJ/mol. A fit to the more limited data set at 400 MPa in Figure 3b gives 300 ± 60 kJ/mol. This experiment is not influenced by dislocation creep since the stress is low (~25 MPa). We conclude that the activation energy for diffusion creep under wet conditions is 375 ± 75 kJ/mol. Thus, for the limited data sets available at this time, the difference in the activation energy for diffusion creep under wet and dry conditions does not appear to be significant.

Activation Energy for Dislocation Creep: Dry Conditions

The activation energy for dislocation creep under dry conditions is constrained by a combination of experiments on single crystals, fine-grained aggregates and coarse-grained natural aggregates. For fine-grained aggregates, only a handful of experiments were specifically designed to measure the activation energy in the dislocation creep regime. A least squares fit to the data from the study of *Mei and Kohlstedt* [2000b] shown in Figure 3c gives E^* = 530 ± 40 kJ/mol. Similar to the analyses discussed above, the component of diffusion creep to the total strain rate was removed prior to the fit. This value is within error of that determined by *Chopra and Paterson* [1984] for coarse-grained natural dunites. Also, the strain rate agrees well with the average strain rate determined at a temperature of 1300°C by *Karato et al.* [1986]. In addition, these values for activation energy are within error of the value of 450 ± 100 kJ/mol determined for fine-grained lherzolite samples [*Zimmerman,* 1999]. A fit to the lower stress data from *Chopra and Paterson* [1984] shown in Figure 3c gives E^* = 550 ± 20 kJ/mol. In this case, data at stresses significantly greater than the confining pressure were omitted due to the possibility that they are influenced by a change in deformation mechanism. For comparison, the flow laws for olivine single crystals deformed on their easiest (i.e., (010)[100]) and hardest (i.e., (010)[001]) slip systems under dry conditions are also shown. As discussed below, the higher strain rates observed in the experiment of *Hirth and Kohlstedt* [1995b] are likely a result of a transition to grain boundary sliding limited by dislocation slip. As illustrated in Figure 3c, the activation energy of 520 ± 110 kJ/mol and the magnitude of the strain rate for this sample are similar to those for the easiest slip system in olivine.

Activation Energy for Dislocation Creep: Wet Conditions

The activation energy for dislocation creep under wet conditions is similar to that determined under dry conditions. A least squares fit to the data of *Mei and Kohlstedt* [2000b] shown in Figure 3d gives E^* = 510 ± 70 kJ/mol. This value is in good agreement with the value of 530 ± 30 kJ/mol[1] determined from data for Anita Bay dunite also plotted in Figure 3d. As discussed by *Hirth and Kohlstedt* [1996], the lower value reported for these samples by *Chopra and Paterson* [1981] results from including high stress data in the fit and an underestimation of the stress exponent. The activation energy determined for the Aheim dunite under wet conditions is significantly smaller than that under dry conditions [see *Hirth and Kohlstedt,* 1996]; the lower value for Aheim dunite (E^* = 310 ± 90 kJ/mol) probably results from a concomitant decrease in the water content of the olivine with increasing temperature due to partial melting of the samples.

Pressure Dependence

One of the largest uncertainties in extrapolating experimental data is the large difference in pressure between laboratory and natural conditions. The highest resolution mechanical data are acquired at ~300 MPa, while the pressure in high-temperature regions of the upper mantle beneath subduction zones are 2-12 GPa. As illustrated in Figure 4a, differences in the activation volume reported in the literature for dislocation creep and dislocation recovery of $V^* = 5\times10^{-6}$ to 27×10^{-6} m^3/mol result in several orders of magnitude uncertainty in the viscosity at the greatest depths in the upper mantle. Over the full depth range in the mantle wedge, the effect of pressure on viscosity can be as large or even larger than the temperature dependence on viscosity. For example, with $V^* = 15\times10^{-6}$ m^3/mol, the change in viscosity from 100 to 400 km resulting from the increase in pressure is more than 4 orders of magnitude, similar to the effect of a 400K change in temperature. As discussed below, the extrapolation of laboratory data for the activation volume for creep under wet conditions is further complicat-

[1]In *Hirth and Kohlstedt* [1996] we reported a value of Q = 515 ± 25 kJ/mol based on an analysis of a different subset of the same data from *Chopra and Paterson* [1981]. The value reported here is lower because we removed several data points determined at stresses ranging from 350 to 400 MPa for consistency with the other analyses reported in this paper.

ed by competing effects of the role of water and pressure, specifically the effect of pressure on the concentration of water in minerals and, hence, on viscosity.

Pressure Dependence Under dry Conditions

The activation volume for dislocation creep under dry conditions has been directly determined by deformation experiments and inferred from dislocation recovery experiments. The resulting values for V^* are listed in Table 2 and plotted in Figure 4b as a function of the maximum pressure tested in each study. The values for V^* determined from deformation experiments are somewhat higher than those determined in recovery studies. In both cases, the data indicate that V^* decreases with increasing pressure.

Similar to the experimental observations in Figure 4b, theoretical treatments predict that the activation volume decreases with increasing pressure. Two general types of relationships have been explored. The first, based on the elastic strain required for creation and migration of point defects, is formulated in terms of the pressure and temperature dependence of elastic moduli. The analysis of *Sammis et al.* [1981] indicates that calculations based on dilatational strain provide a better fit to experimental data than those determined using shear strain. In this case [see *Sammis et al.* [1981] after *Zener* [1942] and *Keyes* [1963]],

$$V^* = E^*[\partial \ln K_T/\partial P)_T - 1/K_T]\times [1 - (\partial \ln K_T/\partial \ln T)_P - \alpha_T T]^{-1} \quad (3)$$

where K_T is the isothermal bulk modulus and α_T is the coefficient of thermal expansion. This relationship, plotted in Figure 4b using elastic constants and derivatives for single crystal olivine [*Kumazawa and Anderson,* 1969], provides a reasonable representation of the experimental deformation data.

Founded on theoretical analyses relating melting temperature and vacancy concentration, and the observation that activation energy increases with increasing melting temperature (T_m), V^* for diffusion has been estimated using the pressure dependence of the melting temperature [e.g., *Weertman,* 1970]. In this case

$$V^* = E^*(\partial T_m/\partial P)/T_m. \quad (4)$$

A modification of this description for V^* has been suggested by Sammis et al. [1981], however, this change only modestly influences V^* for upper mantle conditions. The change in V^* with increasing pressure (depth) determined using this homologous temperature approach is illustrated

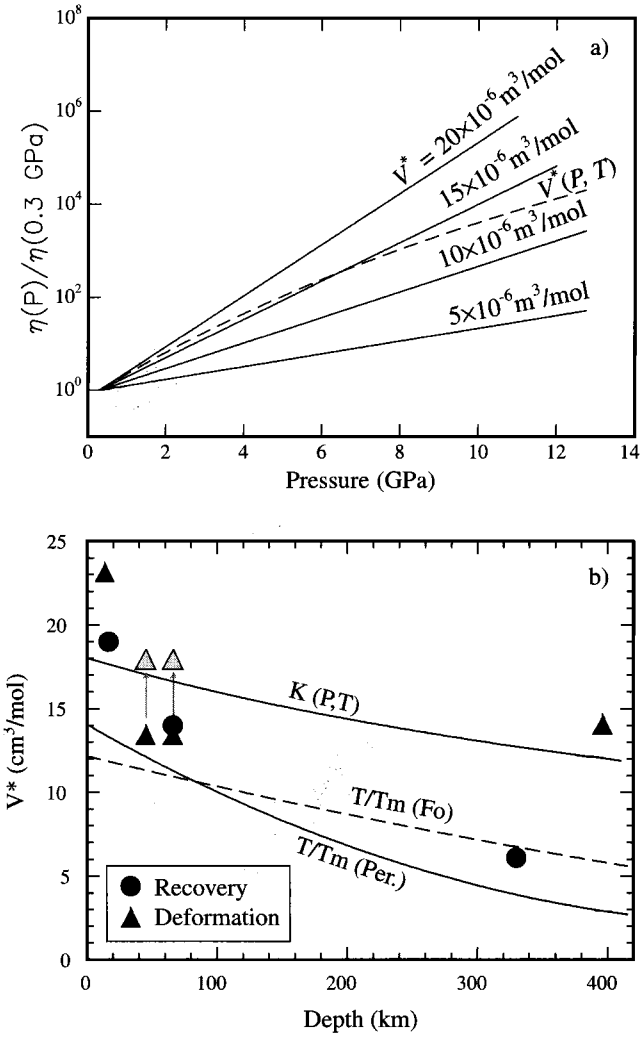

Figure 4. Plots showing the pressure dependence of deformation. (a) Plot of normalized viscosity versus pressure for a temperature of 1350°C and E^* = 530 kJ/mol. The viscosities calculated for constant values of V^* are normalized by the value at 0.3 GPa to emphasize the large effect of pressure on viscosity. The normalized viscosity for a V^* that decreases with increasing pressure ($V^*(P,T)$, calculated using equation 3) is also shown. (b) Comparison of experimental determinations of V^* to theoretical relationships calculated using the pressure and temperature dependence of the bulk modulus ($K(P,T)$ from equation 3) and the effect of pressure on the melting temperature of forsterite (T/Tm (Fo), calculated using equation 4) and the liquidus of peridotite (T/Tm (Per.), calculated using equation 4). The data sources for V^* determined from deformation experiments and recovery experiments are listed in Table 2. As discussed by *Kohlstedt et al.* [1980] an additional uncertainty in V^* arises due to the pressure dependence of thermocouple EMF. The gray symbols and arrows on the deformation data points at 45 and 60 km reflect this uncertainty.

Table 2. Determination of Activation Volumes

Technique	V* (10^{-6} m^3/mol)	P range (GPa)	Reference
Deformation	23	0.2-0.4	*Kohlstedt and Wang* [2001][b]
Deformation	13.4 (18)[a]	0.5-1.5	*Ross et al.* [1979]
Deformation	14 (18)[a]	0.3-2	*Karato and Jung* [2002]
Deformation	14	0.3-15	*Karato and Rubie* [1997]
Deformation	27	0.6-2.0	*Borch and Green* [1989]
Recovery	19[c]	10^{-4}-0.5	*Kohlstedt et al.* [1980]
Recovery	14	10^{-4}-2.0	*Karato and Ogawa* [1982]
Recovery	6	10^{-4}-10	*Karato et al.* [1993]
Diffusion (Si)	-2	5-10	*Bejina et al.* [1997]

[a]Higher value is corrected for pressure effect on thermocouple emf.
[b]Also, *Wang et al.*, Activation volume for dislocation creep in olivine (manuscript in preparation).
[c]Corrected value from *Karato* [1981].

in Figure 4b by using the pressure dependence on the melting temperature of forsterite [*Ohtaini and Kumazawa,* 1981] and the liquidus of lherzolite [*Zhang and Herzberg,* 1994]. We used the liquidus temperature of lherzolite to approximate the solidus of Fo_{88} olivine at high pressure. We emphasize that the appropriate scaling for the homologous temperature approach is to use the melting point of the mineral grains, instead of the eutectic melting point of the rock. To underscore this point, note that the creep rate of partially molten dunite with a melt fraction of <1% is approximately the same as the creep rate of single crystal olivine even though the solidus of the partially molten aggregate (~1100°C) is significantly lower than that of the olivine (~1800°C) [*Hirth and Kohlstedt,* 1995b].

The lower values of V^* at high pressure determined using the recovery experiments are similar to those predicted using the homologous temperature approach (Figure 4b). In general both the deformation and recovery data are reasonably bracketed using the theoretical treatments. While the agreement between the homologous temperature approach and the recovery data is encouraging, we note that microstructural observations suggest that climb is not the limiting process for creep on (010)[001], the hardest slip system in olivine [*Bai and Kohlstedt,* 1992]. Based on the von Mises criterion, the hardest slip system is expected to limit deformation during dislocation creep [*Paterson,* 1969].

Surprisingly, the activation volume determined for Si self-diffusion in olivine, $V^* = 1.9\times10^6 \pm 2.4\times10^{-6}$ m^3/mol [*Bejina et al.,* 1997], is considerably lower than that observed for recovery. The essentially negligible effect of pressure is consistent with values of D_{Si} determined at ambient pressure by *Houlier et al.,* [1990] and *Dohman et al.* [2002]. Since silicon is the slowest diffusing species in olivine, it is expected to limit the rate of dislocation climb. However, the rate of climb determined from recovery experiments is several orders of magnitude greater than that expected based on the experimental data for D_{Si}. Climb requires diffusion on distances comparable to the dislocation spacing (i.e., between 50 to 500 nm for experimental samples). Given $D_{Si} = 5\times10^{-21}$ m^2/s at 1300°C [*Houlier et al.,* 1990], diffusion distances for Si over times of 0.01-1 hour are on the order of 0.4-4 nm. By contrast, experimental observations from both deformation experiments [e.g., *Mackwell et al.,* 1985] and recovery experiments [e.g., *Goetze and Kohlstedt,* 1973] demonstrate considerable dislocation climb over the same time periods. Interestingly, the rates of climb do correspond well with the rate of oxygen diffusivity [e.g., *Ryerson et al.,* 1989; *Dohman,* 2002], which are approximately two orders of magnitude greater than D_{Si} at experimental conditions. However, the activation energy for oxygen diffusion is considerably smaller than that observed for creep.

The large difference between the activation volume for D_{Si} and that for recovery, together with the discrepancy between D_{Si} and the rate of recovery, suggests that dislocation climb in olivine is not limited by matrix diffusion of silicon. As suggested above, one explanation for this apparent discrepancy is that climb is limited by oxygen matrix diffusion. In this case, the effective diffusion rate for silicon must be greater than that for oxygen matrix diffusion, indicating that silicon may diffuse primarily along dislocation cores (i.e., pipe diffusion). Alternatively, climb could be limited by silicon pipe diffusion. Interestingly, if deformation is limited by pipe diffusion, the Orowan equation predicts that the $\dot{\varepsilon} \propto v\rho^2$ [e.g., *Frost and Ashby,* 1982], where v, the dislocation velocity (i.e., climb velocity), is proportional to σ and ρ is the dislocation density. In general, $\rho \propto \sigma^q$, where q is often assumed to be 2 based on simple dislocation geometries. However, for olivine $\rho \propto \sigma^{1.37}$ [*Bai*

and Kohlstedt, 1992], thus giving , $\dot{\varepsilon} \propto \rho^{3.7}$ which is within error of that determined from experimental studies for olivine (see above).

In practical determinations of the activation volume it is important to account for the potential change in V^* with increasing pressure. Specifically, because

$$V^*(P) = -(\partial \ln\dot{\varepsilon}/\partial P)RT + P\partial V/\partial P, \quad (5)$$

then $V^*(P) = -(\partial \ln\dot{\varepsilon}/\partial P)RT$ only if $\partial V/\partial P = 0$. However, since V^* apparently decreases with increasing pressure, determining $(\partial \ln\dot{\varepsilon}/\partial P)RT$ at high pressure underestimates V^*, unless the data are compared to similar data at low pressure. This problem can be seen in Figure 4a, where the pressure dependence of viscosity predicted by equation (3) is plotted versus pressure. Note that the slope of the relation at high pressure is significantly smaller than that predicted for the constant values of V^*. In practice, V^* in equation 1 is a "chord V^*", representing $RT[(\ln\dot{\varepsilon})_P - (\ln\dot{\varepsilon})_{P=0}]/P$. The values for V^* shown in Table 1 for which the pressure range extends to 1 atm (i.e., 1×10^{-4} GPa) provide a good approximation for the chord V^*.

There are limited constraints on the activation volume for diffusion creep under dry conditions. The comparison of diffusion creep data on samples deformed at 1 atm and 300 MPa gives a value in the range of 2×10^{-6} to 10×10^{-6} m^3/mol [*Kohlstedt et al.,* 2000]. The range given here reflects uncertainties associated with the correction for cavitation during creep at ambient pressures.

Combined Water and Pressure Dependence Under wet Conditions

Under water-saturated conditions, an increase in pressure influences creep rates in two ways. First, there is a direct effect: creep rates decrease due to an activation volume effect. Second, there is an indirect effect: creep rate increases with increasing pressure because (a) the solubility of water in nominally anhydrous minerals increases with increasing water fugacity [*Kohlstedt et al.,* 1996], (b) water fugacity increases with increasing pressure for a fixed water activity, and (c) creep rates increase with increasing water content [e.g., *Mei and Kohlstedt,* 2000a,b]. Following *Mei and Kohlstedt* [2000a,b] and *Karato and Jung* [in press], we show a least squares fit to experimental data for samples deformed under water-saturated conditions at various pressures (Figure 5a). The fit to the global data set (excluding the results of *Borch and Green,* 1989[2]) gives values of the water fugacity exponent of $r = 1.2 \pm 0.4$ and $V^* = 22 \pm 11$.

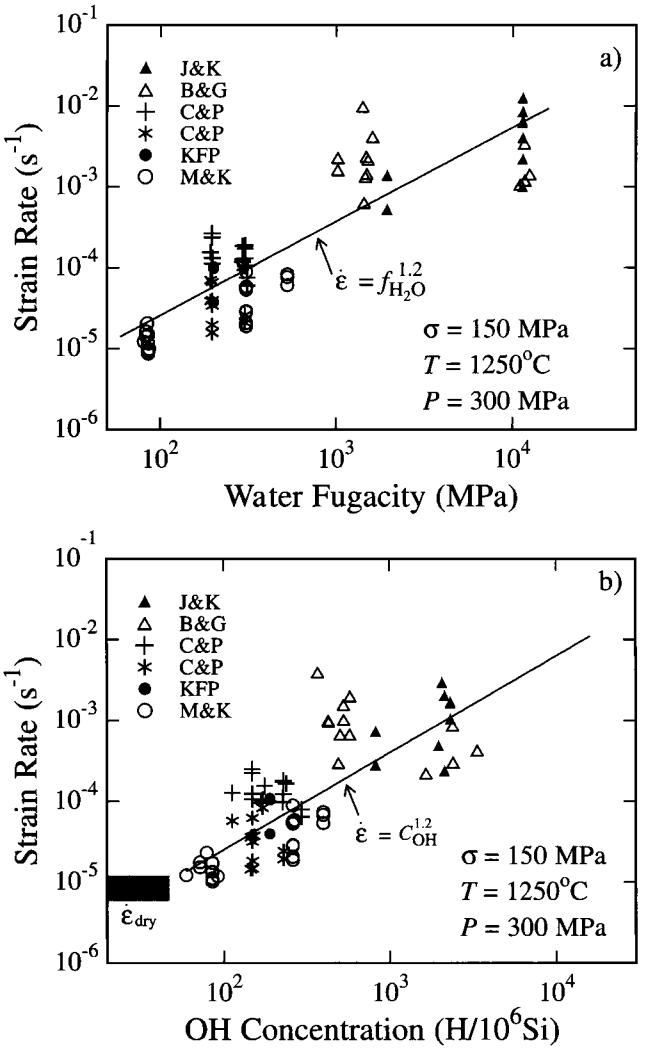

Figure 5. Plots of strain rate versus water fugacity (a) and water content (b) for olivine aggregates deformed in the dislocation creep regime. The data are normalized to a pressure of 300 MPa using the value of V^* determined from a non-linear fit to the global data set after the data were normalized to a constant stress and temperature using $n = 3.5$ and $E^* = 520$ kJ/mol. The strain rate determined under dry conditions at the same temperature and stress is shown by the shaded box in 5b. J&K = *Jung and Karato* [2001]; B&G = *Borch and Green* [1989]; C&P = *Chopra and Paterson* [1984]; KFP = *Karato et al.* [1986]; M&K = *Mei and Kohlstedt.*

[2]The results of *Borch and Green* [1989] are not included in the fit shown in Figure 5a because the water content in their samples was not controlled. As discussed in *Hirth and Kohlstedt* [1996], although *Borch and Green* [1989] reported that their samples were dry, subsequent FTIR analyses [*Young et al.,* 1993] showed that they may have contained enough water to saturate olivine at 1.0 GPa.

As suggested by Karato and Jung [in press], the higher-pressure data can improve the resolution of the competing effects of water fugacity and activation volume.

Following *Hirth and Kohlstedt* [1996] and *Karato* [this volume], for geodynamic applications it is more practical to consider how strain rate changes with increasing water content rather than increasing water fugacity. Based on the hypothesis that water influences creep rate due to its effect on point defect concentrations [e.g., *Mackwell et al.,* 1985; *Kohlstedt and Mackwell,* 1998], the influence of water on creep rate should depend on water content even when $a_{H_2O} < 1$. In Figure 5b we plot strain rate versus water content for the same data used in Figure 5a. The water concentration (C_{OH}) is calculated for Fo_{90} olivine using the relationship [*Kohlstedt et al.,* 1996; Zhao, Y.-H., S.B. Ginsberg, and D.L. Kohlstedt, Solubility of Hydrogen in Olivine: Dependence on Temperature and Iron Content, in prep.]

$$C_{OH} = A_{H2O} \exp[-(E_{H2O} + PV_{H2O})/RT] f_{H2O} \qquad (6)$$

where A_{H2O} = 26 H/10^6 Si/MPa, E_{H2O} = 40 kJ/mol, V_{H2O} = 10×10^{-6} m^3/mol and f_{H2O} is water fugacity in MPa. The strain rate determined under dry conditions at the same temperature and stress is also shown in Figure 5b. The least squares fit in Figure 5b intersects the dry strain rate value at a water content of approximately 50 H/10^6Si. This observation, and the fact that strain rate increases approximately linearly with increasing water concentration, is consistent with the point defect hypothesis [*Mei and Kohlstedt,* 2000b]. At water contents below ~50 H/10^6Si, the charge neutrality condition, which controls the concentration of point defects, changes and the creep rate is controlled by the same process as that observed for dry conditions. The water concentrations shown in Figure 5b are based on the *Paterson* [1982] relationship between FTIR absorbance and C_{OH}. These values may underestimate actual water contents by as much as a factor of 3 [*Bell et al.,* 2002]. In terms of the flow law, the *Bell et al.* [2002] calibration does not change the dependence of creep rate on water content, however, the pre-exponential constant would decrease by a factor of three.

Experimental studies also demonstrate that creep rates in the diffusion creep regime increase with increasing water content [e.g., *Mei and Kohlstedt,* 2001a]. The effect of water fugacity or water content on deformation in the diffusion creep regime has been determined by conducting experiments under water-saturated conditions as a function of pressure [*Mei and Kohlstedt,* 2000a]. The results of these experiments are consistent with the power law formulation for the effect of strain rate on water fugacity illustrated by equation 1. The value of the water fugacity exponent (r) in the diffusion creep regime is 1.0±0.3. As discussed by Mei and Kohlstedt (2001a), the uncertainty in r is again related to the concomitant effect of the PV^* term in equation 1 on strain rate. *Mei and Kohlstedt* [2000a] concluded that the effect of water on creep rate in the diffusion creep regime arises due to the influence of water fugacity on the concentration of point defects in the grain boundaries. This conclusion is consistent with the observation that the values for n, p and E^* in the diffusion creep regime are similar under wet and dry conditions.

Grain Boundary Sliding

Dislocation creep is generally assumed to be independent of grain size. However, at conditions near the transition from diffusion creep to dislocation creep, strain rates for dry olivine aggregates in the dislocation creep regime increase with decreasing grain size. This grain size effect is illustrated in Figure 6a, together with flow laws for olivine single crystals. As shown in Figure 6b, there is no discernable grain size dependence for dislocation creep under hydrous conditions.

Based on the observation that creep rates for fine-grained olivine aggregates are similar to the strain rates of olivine single crystals deformed on the easiest slip system, *Hirth and Kohlstedt* [1995b] concluded that these samples deformed by grain boundary sliding (GBS) accommodated by a dislocation creep process. This hypothesis is further supported by the relatively large influence of melt on creep rate, the lack of grain flattening observed in the largest grains, and the observation that the GBS process is observed near the transition between dislocation creep and diffusion creep. Grain boundary sliding is implicit at these conditions because of the necessity for GBS in the diffusion creep regime [*Raj and Ashby,* 1971]. Constitutive laws for dislocation accommodated GBS are of the form $\dot{\varepsilon} \propto \sigma^n / d^p$, where $n_{gbs} \approx 2$ to 3 and $p_{gbs} \approx 2$ to 1 [e.g., *Langdon,* 1994]. To explore the grain size sensitivity in the GBS regime, we plot strain rate versus grain size in Figure 7a. The contribution of diffusion creep to the total strain rate of these samples has been removed using the fitting procedures described in the section on stress dependence. The stress exponent for these samples is $n = 3.5 \pm 0.3$ (Figure 2c). For grain sizes between 10 and 60 μm, the data indicate a grain size exponent between 1 and 2. Recent experiments in which creep rate is observed to decrease during grain growth of individual samples indicate a grain size exponent in the GBS regime of $p = 1.8 \pm 0.2$ [*Kohlstedt and Wang,* 2001]. No difference in creep rate is observed between natural dunite samples with a grain sizes of 100 μm and those with a grain size of 900 μm.

The identification of GBS for olivine is complicated since $n_{gbs} \approx n_{disl}$. In this case, a transition from one mechanism to the other will occur with a change in grain size, but not with a change in stress. This scenario is illustrated schematically in plots of strain rate versus differential stress for different grain sizes in Figures 7b-7d using the constitutive law

$$\dot{\varepsilon} = \dot{\varepsilon}_{disl} + \dot{\varepsilon}_{diff} + [1/\dot{\varepsilon}_{gbs} + 1/\dot{\varepsilon}_{easy}]^{-1} \quad (7)$$

with $n_{gbs} = 3.5$ and $p_{gbs} = 2$. A key feature of this constitutive law, which was motivated by similar data for deformation of fine-grained ice [*Goldsby and Kohlstedt,* 2001; *Durham et al.,* 2001], is that GBS and slip on the easiest slip system ($\dot{\varepsilon}_{easy}$) are both required to accommodate deformation. Based on these observations, we conclude that the importance of GBS under geologic conditions can be explored by extrapolating the strain rates for diffusion creep, dislocation creep of coarse-grained aggregates and dislocation creep of olivine on its easiest slip system. As summarized in Table 1, we assume that E^*_{gbs} is the same as that for dislocation creep of olivine on its easiest slip system.

The lack of grain size dependence for dislocation creep processes under wet conditions and the observation that creep rates even in the coarse-grained natural samples are similar to the easiest slip systems suggests that von Mises criterion is satisfied without slip on the hardest slip system. One explanation for these observations is that, to meet compatibility requirements, a significant amount of strain occurs by dislocation climb under hydrous conditions. Climb accommodates as much as 10% strain at high temperatures under dry condition [*Durham and Goetze,* 1977]. Microstructural observations suggest that even more strain is accommodated by climb under hydrous conditions [e.g., *Mackwell et al.,* 1985]. Hence, under hydrous conditions, dislocation climb apparently accommodates the strain that is accommodated by either GBS or slip on the hardest slip system under dry conditions.

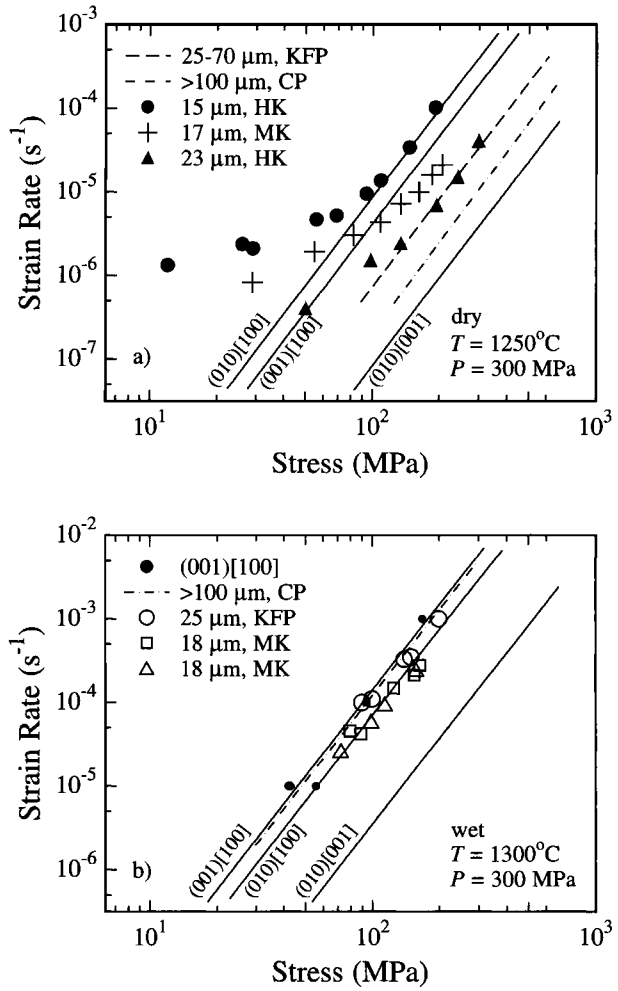

Figure 6. Plots of strain rate versus differential stress for olivine aggregates with different grain sizes deformed under dry and wet conditions. (a) Under dry conditions, at a constant stress, the strain rate in the dislocation creep regime increases with decreasing grain size. This observation suggests that creep of the fine-grained olivine aggregates occurs by dislocation-accommodated grain boundary sliding. For the finest-grained samples, a transition to diffusion creep is illustrated with decreasing differential stress. (b) Under wet conditions, there is no apparent effect of grain size on strain rate. Creep rates for olivine single crystals deformed in orientations to promote slip on different slip systems under dry [*Bai et al.,* 1991] and wet [*Mackwell et al.,* 1985] conditions are also shown. KFP = *Karato et al.* [1986]; C&P = *Chopra and Paterson* [1984]; H&K = *Hirth and Kohlstedt,* 1995; M&K = *Mei and Kohlstedt.*

Influence of melt content

The role of melt on the creep properties of mantle aggregates has been studied extensively during the last 15 years. We will not review the results of these studies in detail here; readers are referred to recent review articles on the subject [*Kohlstedt et al.,* 2000; *Xu et al.,* 2002]. For the purposes of this paper, we summarize the experimental data for the influence of melt fraction (ϕ) on strain rate in Figure 8. For both wet and dry conditions, the data at $\phi \leq 0.12$ are well described by an exponential relationship $\dot{\varepsilon} \propto \exp(\alpha\phi)$, where α is a constant between 25-30 for the diffusion creep regime and between 30-45 for the dislocation creep regime. For a given stress, this relationship can also be written $\eta \propto \exp(-\alpha\phi)$, where η is effective viscosity. Analyses of data for partially molten lherzolites with pyroxene contents as high as 35% indicate a more modest effect of melt on strain

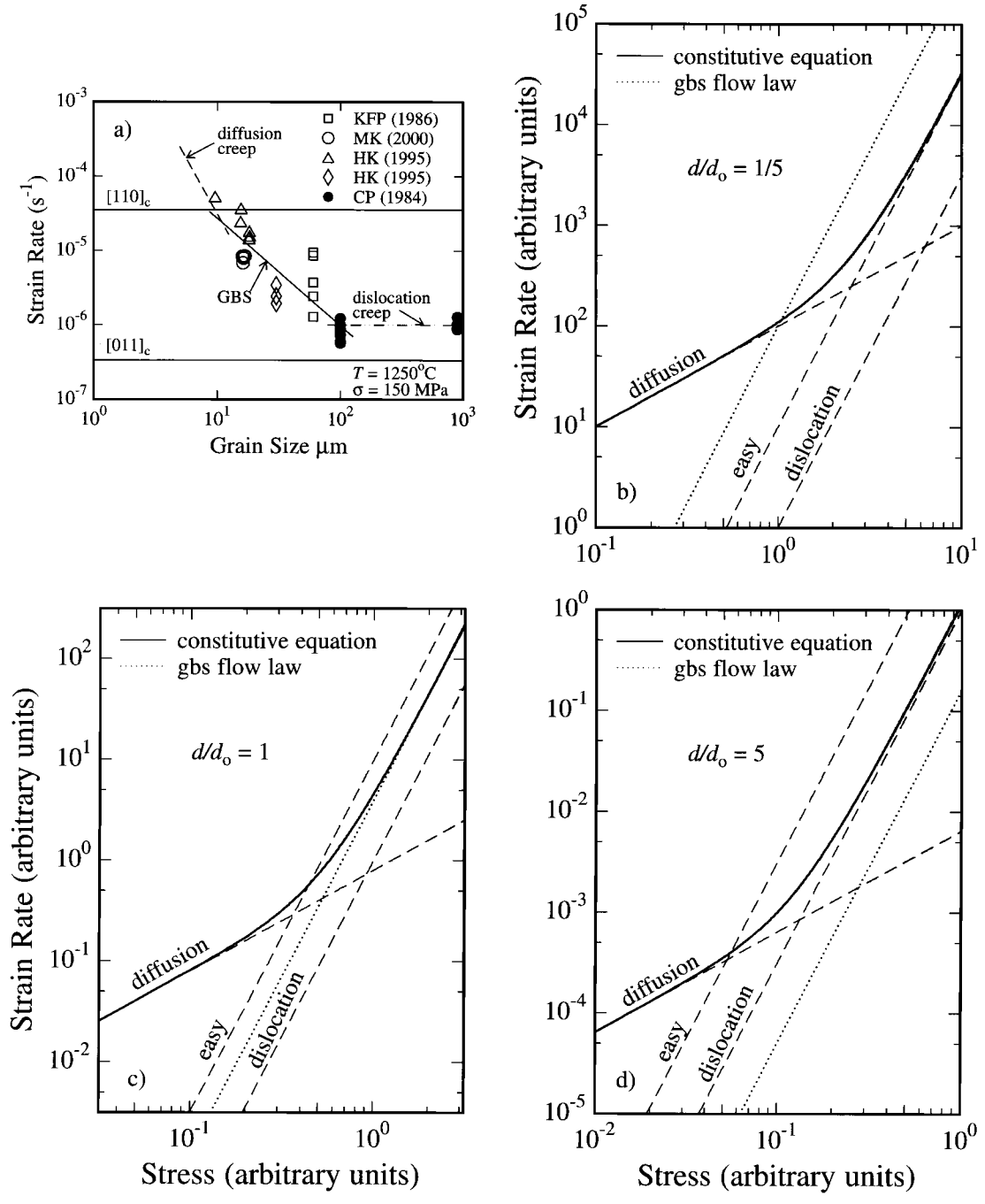

Figure 7. Plots of strain rate versus grain size. (a) Plot showing the effect of grain size on strain rate for fine-grained olivine aggregates deformed in the dislocation creep regime. The data are normalized to a constant stress using $n = 3.5$ after the component of diffusion creep to the total strain rate is subtracted (e.g., see Figure 2). A linear fit to the data over the grain size interval of 10-60 μm (labeled GBS) gives a grain size exponent of $p \approx 2$, consistent with models for dislocation-accommodated GBS. For comparison, flow laws for diffusion creep, dislocation creep of coarse-grained olivine and olivine single crystals are also shown. (b-d) Schematic plots of strain rate versus grain size calculated using equation 7 illustrating how transitions between the deformation mechanisms occur with changes in grain size. The units of stress and strain rate in Figures 7b-7d are arbitrary.

rate [*Zimmerman,* 1999]. The exponential relationship still provides a good fit to the data, but the constant α is ~20 in the diffusion creep regime and ~25 in the dislocation creep regime. One explanation for this difference between dunite and lherzolite samples is that the presence of pyroxene reduces the amount of grain boundary area wetted by melt. Thus, because the melt does not support shear stress, the effective stress for partially molten lherzolite is smaller than that for partially molten dunite at the same melt fraction. Experimental observations indicate that basaltic melt does not wet pyroxene-pyroxene grain boundaries as effectively as olivine-olivine grain boundaries [*Toramaru and Fujii,* 1986; *Daines and Kohlstedt,* 1993].

The exponential relationship between strain rate and melt fraction is empirical. For the diffusion creep regime, the effect of melt on creep rate is significantly greater than that predicted by theoretical treatments in which melt topology is assumed to be controlled by isotropic interfacial energies [*Cooper et al.,* 1989]. The enhanced strain rates are explained by deviations from ideal melt topologies that arise due to anisotropic interfacial energies [e.g., *Hirth and Kohlstedt,* 1995a; *Mei et al.,* 2002] and changes in grain coordination with increasing melt fraction [*Renner et al.,* 2002]. The reader is referred to these studies for more detailed analyses.

The dependence of melt fraction on strain rate in the dislocation creep regime is also much greater than predicted by theoretical models. The effect of melt fraction on strain rate for partially molten dunite suggests that $\dot{\varepsilon} \propto (\sigma_{eff})^n$, where $\sigma_{eff} \propto \sigma/(1-x)$ and x is the fraction of grain boundary area replaced by melt [*Hirth and Kohlstedt,* 1995b; *Mei et al.,* 2002]. This relationship emphasizes the importance of grain boundary stresses during creep and suggests the potential importance of GBS in the dislocation creep regime. An intriguing possibility is that the presence of melt may promote dislocation accommodated GBS, resulting in a relaxation of the von Mises criterion. If so, a significant decrease in viscosity could arise due to the presence of melt fractions as small as ~1%. A key factor for developing these ideas is the determination of the influence of melt on strain rate for coarse-grained olivine aggregates. This sort of study is somewhat tricky, due to the problem of maintaining "textural equilibrium" at the relatively high strain rates necessary in laboratory experiments.

In conclusion, our understanding of the effects of melt on the rheology of partially molten peridotite is continuing to improve. For example, an important problem that will receive continued attention over the next few years is understanding the relationships between grain scale melt redistribution and viscosity [e.g., *Renner et al.,* 2000; *Holtzman et al.,* 2002]. At present, while more sophisticated analyses have been presented by us and others, for practical reasons we conclude that the exponential relationships between melt fraction and strain rate/viscosity shown in Figure 8 for $\phi \lesssim 0.12$ are appropriate first-order approximations for application in geodynamic models.

EXTRAPOLATION OF EXPERIMENTAL DATA TO THE OCEANIC MANTLE AND THE MANTLE WEDGE

In this section we examine predictions for the viscosity of the oceanic mantle and the mantle wedge based on extrapolation of laboratory data. In addition, we compare these experimental constraints with independent geophysical estimates for upper mantle viscosity. Because viscosity is likely to be stress-dependent in at least some parts of the upper mantle (i.e., dislocation creep is the dominant deformation mechanism), we first illustrate the importance of assumptions about stress and strain rate conditions on the effects of temperature and pressure on viscosity, and then compare these results to approximations sometimes used in numerical studies of mantle convection.

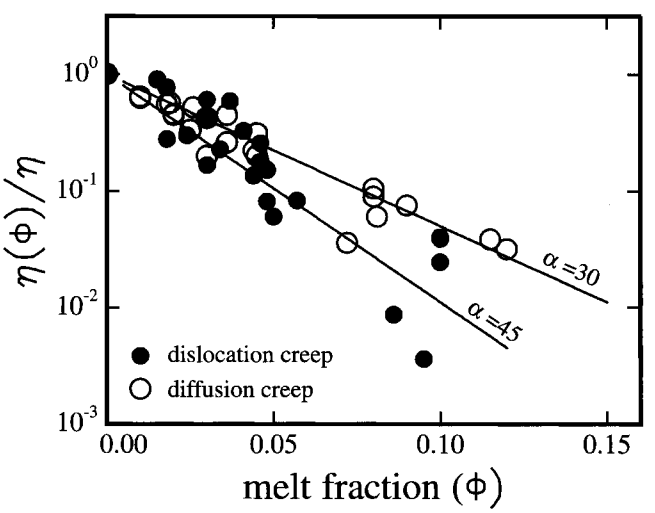

Figure 8. Plot of normalized viscosity versus melt fraction for olivine aggregates deformed in the diffusion creep and dislocation creep regimes. For each data point, the viscosity is normalized by the viscosity of a melt-free aggregate deformed at the same conditions. For both deformation regimes, the exponential relationship $\eta \propto \exp(-\alpha\phi)$ provides a good first-order approximation for the decrease in viscosity with increasing melt fraction with values of α ranging from 30-45. Data are from the studies of *Cooper and Kohlstedt* [1984], *Beeman and Kohlstedt* [1993], *Hirth and Kohlstedt* [1995a,b], *Kohlstedt and Zimmerman* [1996], *Bai et al.* [1997], *Gribb and Cooper* [2000] and *Mei et al.* [2002].

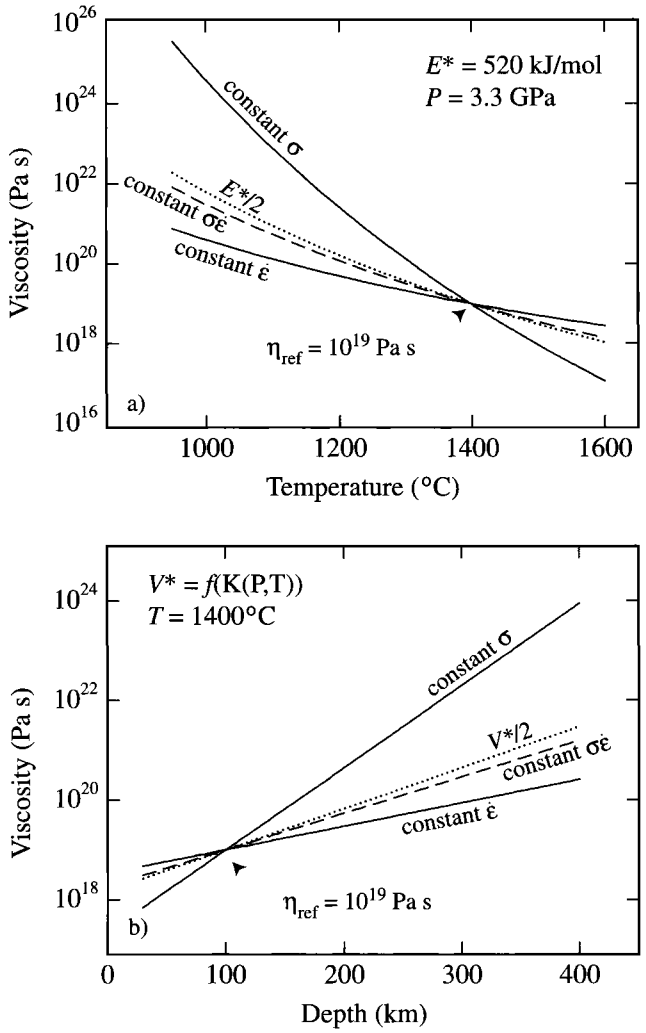

Figure 9. Plots illustrating the effects of temperature and pressure on stress-dependent viscosity. (a) Plots showing the variation in viscosity with changing temperature at a pressure of 3.3 GPa calculated relative to a reference viscosity of 10^{19} Pa s using E^* = 520 kJ/mol for a constant $\dot{\varepsilon}$, constant σ and constant $\dot{\varepsilon}\sigma$. The influence of temperature calculated for a stress-independent viscosity with E^* = 260 kJ/mol (labeled $E^*/2$) is shown for comparison. (b) Plots of the variation in viscosity with increasing depth (pressure) calculated using equation 3 for V^* at a constant temperature of 1400°C.

Temperature and Pressure Dependence of Non-linear Viscosity

The relatively large values of E^* and V^* for dislocation creep indicate that the viscosity of the upper mantle is strongly dependent on temperature and pressure. For example, at upper mantle temperatures under constant stress conditions, a change in temperature of only 30 K results in a factor of two change in viscosity for E^* = 520 kJ/mol. Similarly, viscosity decreases an order of magnitude with a 100 K increase in temperature. However, when applying dislocation creep flow laws to mantle conditions, it is important to consider whether deformation occurs closer to constant stress or to constant strain rate conditions [e.g., *Christensen,* 1989]. As illustrated in Figure 9, the pressure and temperature dependences of viscosity are much greater at a constant stress than at a constant strain rate. Theoretical treatments suggest that the viscosity of convecting systems may evolve such that deformation occurs at a constant rate of viscous dissipation (constant $\dot{\varepsilon}\sigma$) [e.g., *Christensen,* 1989], which results in temperature and pressure effects intermediate between the end-member conditions (Figure 9). The temperature and pressure effects on viscosity at constant $\dot{\varepsilon}\sigma$ are also well fit by assuming that viscosity is independent of stress (i.e., a linear relationship between stress and strain rate) and decreasing both E^* and V^* by a factor of ~2 [*Christensen,* 1989]. This procedure has been employed in modeling studies [e.g., *Braun et al.,* 2000; *Toomey et al.,* 2002] due to numerical instabilities that arise for fully non-linear viscosity formulations in problems with large variations in temperature and pressure.

Viscosity Profiles for the Oceanic Mantle and Mantle Wedge

In Figure 10, we plot the viscosity of the upper mantle as a function of depth predicted by extrapolation of experimental flow laws. Viscosity profiles for adiabatic oceanic mantle are shown in Figure 10a for dislocation creep of olivine with a water content of 1000 H/10^6Si, stresses of 0.1 and 1.0 MPa and a potential temperature of 1350°C. To calculate the viscosity profiles for a constant water content, we decreased the activation parameters to account for the temperature and pressure dependence on water content in olivine (i.e., $E^*_{eff} = E^* - E_{H2O}$ and $V^*_{eff} = V^* - V_{H2O}$), where E_{H2O} and V_{H2O} are the values from Equation (6) [*Mei and Kohlstedt,* 2000b, *Karato and Jung,* in press]. We use a water content of 1000 H/10^6Si based on the study of *Hirth and Kohlstedt* [1996]; flow law parameters calculated for a constant water content are listed in Table 1.

As discussed above, uncertainty in the value of V^* causes a large uncertainty in the absolute value of mantle viscosity. The profiles in Figure 10a are calculated using V^* determined from Equation 3 to account for the increase in V^* with increasing pressure; the value for V^* calculated from Equation (3) is within error of that determined from the fit in Figure 5. For practical reasons, it is easier to run numerical experiments using a constant value of V^*. As shown in Figure 10a, a value of $V^* = 11\times10^{-6}$ m^3/mol

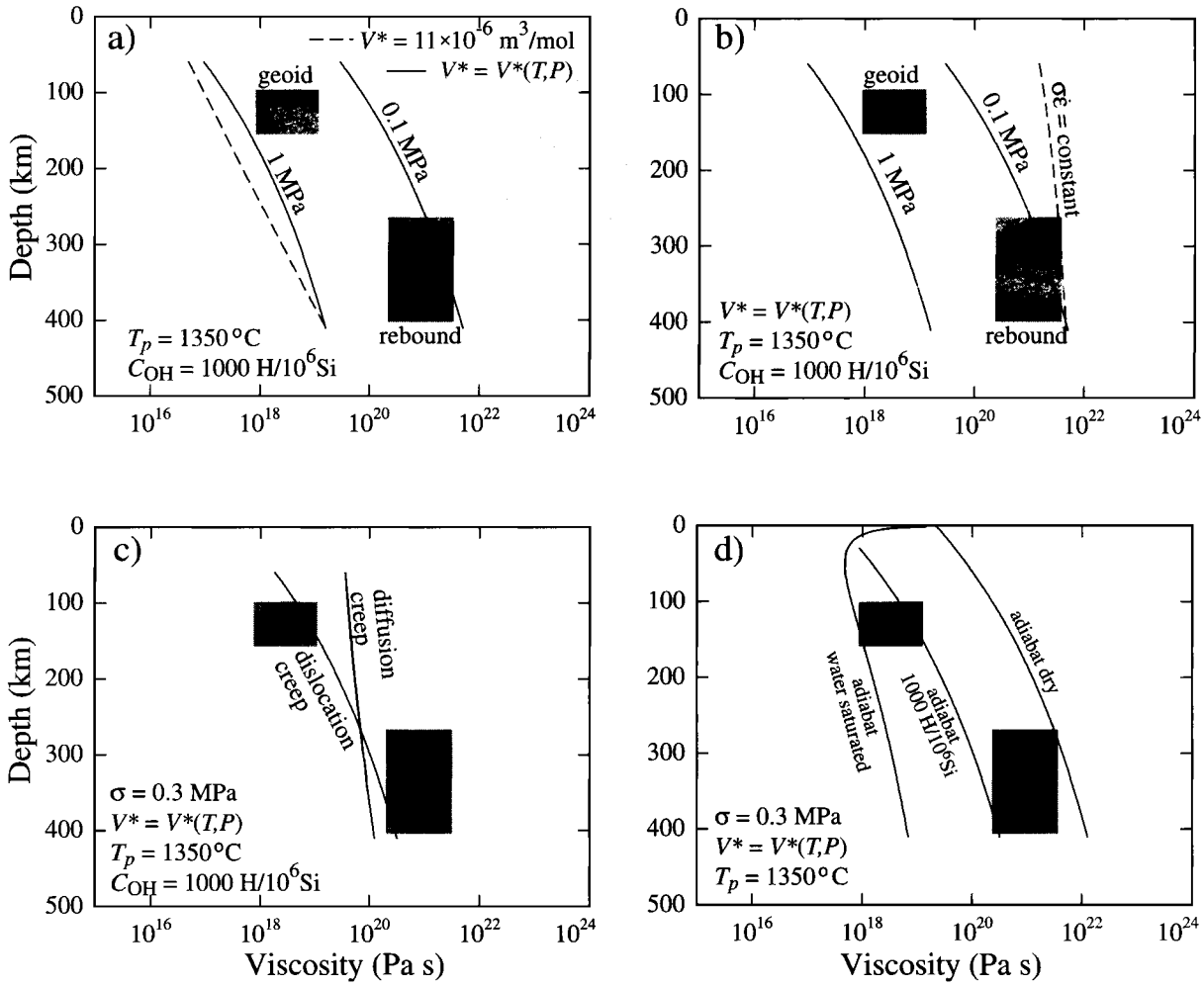

Figure 10. Plots of viscosity versus depth for the upper mantle. (a) Viscosity profiles for adiabatic mantle with a potential temperature of 1350°C. The solid lines show viscosities predicted for dislocation creep of olivine at stresses of 0.1 and 1 MPa with a water content of 1000 H/10^{6}Si and V^* from equation 3. The dashed line shows the viscosity for a constant $V^* = 11\times10^{-6}$m^3/mol. Geophysical estimates for mantle viscosity determined from analyses of the geoid and postglacial rebound are also shown. (b) The same plot as Figure 10a with the addition of the viscosity predicted for constant $\dot{\varepsilon}\sigma$. (c) Viscosity profiles for dislocation creep calculated for a constant stress of 0.3 MPa and diffusion creep assuming a grain size of 10 mm. (d) Viscosity profiles calculated for water-saturated conditions compared with profiles calculated for dry conditions and for a constant water content of 1000 H/10^{6}Si.

provides a relatively good fit to the profile calculated assuming a pressure-dependent V^* and also agrees with the fit in Figure 5. The large difference in the magnitude of viscosity calculated for stresses of 0.1 and 1.0 MPa emphasizes the uncertainty in accuracy (as opposed to precision) associated with extrapolation of the dislocation creep flow laws to asthenospheric conditions.

The change in viscosity with depth predicted for the constant stress viscosity profiles is similar to that suggested by independent geophysical estimates (Figure 10). Based on analysis of the geoid, the viscosity of the oceanic mantle asthenosphere is $\leq 2\times10^{19}$ Pa s [*Craig and McKenzie,* 1986; *Hager,* 1991]. The numerical models presented by *Craig and McKenzie* also indicate that the relatively low viscosity asthenosphere must be restricted to depths less than ~200 km. At the base of the olivine stability field (i.e., at depths above the α–β transition) a viscosity of ~10^{21} Pa s is estimated by the analysis of post-glacial rebound [e.g., *Peltier,* 1998]. The applicability of the rebound viscosity to the oceanic mantle is suggested by the similarity of seismic velocity [e.g., *Gaherty and Jordan,* 1995] and electrical conductivity [e.g., *Hirth et al.,* 2000] for oceanic mantle and

sub-continental mantle at depths between ~300-400 km. A relatively large increase in viscosity with depth in the upper mantle is also suggested by some joint inversions of geoid and dynamic topography data [*Panasyuk and Hager,* 2000].

For comparison with the geophysical estimates, the depth dependence of viscosity predicted for constant $\dot{\varepsilon}\sigma$ is shown in Figure 10b. As suggested by Figure 9, the change in viscosity with depth (i.e., pressure and temperature) calculated with a constant value of $\dot{\varepsilon}\sigma$ is considerably smaller than that calculated assuming a constant stress and is also considerably smaller than that suggested by the geophysical constraints. At face value, this observation is inconsistent with the notion that convecting systems evolve to a condition of constant viscous dissipation. A possible explanation for this apparent discrepancy is that small-scale convection at the base of the plate results in an increase in strain rate (and therefore stress) and a concomitant decrease in viscosity.

Based on the observation that seismic anisotropy is often limited to the upper 200-250 km of the mantle, *Karato* [1992] suggested that a transition from dislocation creep to diffusion creep may occur with increasing depth. The depth at which a transition to diffusion creep occurs is strongly dependent on the grain size in the mantle and the activation volume for diffusion creep. The grain size in the upper mantle is influenced by a number of factors, including dynamic recrystallization and grain growth [e.g., *Karato,* 1984; *Evans et al.,* 2001]. A combination of microstructural studies [e.g., *Ave Lallement et al.,* 1980] and theoretical considerations [*Evans et al.,* 2001] suggests that the grain size in the upper mantle is in the range of 10 mm. The viscosity profile for a grain size of 10 mm plotted in Figure 10c indicates a transition to diffusion creep occurs at a depth of ~250 km if V^* for diffusion creep is ~4×10^{-6} m^3/mol, which is within the bound of 0-20×10^{-6} m^3/mol determined experimentally [*Mei and Kohlstedt,* 2000a]. Recalling the discussion above, the large uncertainty in V^* for diffusion creep at a fixed water activity is due to the competing effects of pressure on creep rate under wet conditions. For all values of V^*, the grain size must be considerably smaller the 10 μm for diffusion creep to be the dominant deformation mechanism at depths of ~100 km.

An important caveat to the hypothesis that a transition to diffusion creep occurs with increasing depth is that grain size tends to evolve toward a value where both deformation mechanisms accommodate the same strain rate [e.g., *de Bresser et al.,* 2001]. Thus, unless grain growth is kinetically inhibited (e.g., by second phase pinning), a complete transition to diffusion creep will not occur.

To illustrate the maxium effect of water on the viscosity of the mantle, we show a viscosity profile for water-saturated olivine aggregates with an adiabatic geotherm in Figure 10d. We use equation 6 to calculate the water content of olivine. For comparison, we also show viscosity profiles for dry olivine on an adiabatic geotherm. A minimum viscosity of 5×10^{17} Pa s for water-saturated conditions occurs at a depth of ~50 km. As discussed above, there are competing effects of pressure on viscosity under water-saturated conditions. At depths shallower than ~50 km, the viscosity increases because the water-content decreases with decreasing pressure and the product PV^* becomes small relative to E^*, such that the decrease in temperature with decreasing depth has a greater effect on viscosity than the decrease in pressure. At depths greater than 50 km, the viscosity increases because the PV^* term dominates over the effects of both increasing water content and increasing temperature.

A possible range of viscosity in the mantle wedge beneath subduction zones is illustrated in Figure 11. One bound on the viscosity is shown by a profile calculated with a geotherm defined by the vapor-saturated solidus at a constant strain rate of 10^{-15} s^{-1}. The lower bound on viscosity is shown by the profile calculated for water-saturated

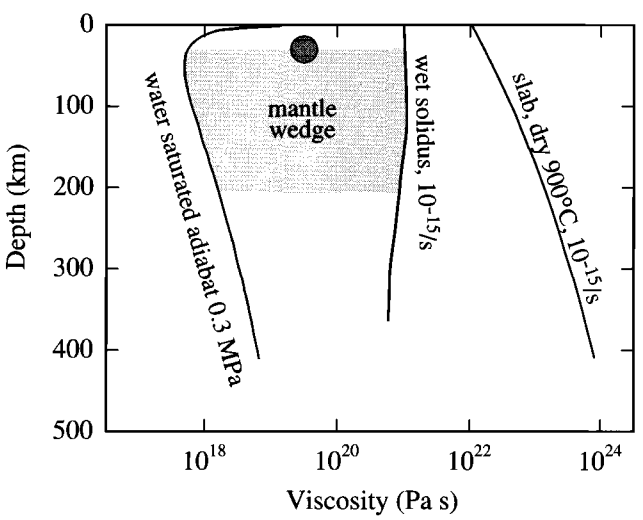

Figure 11. Possible range of viscosity in the mantle wedge. The low viscosity predicted for a depth of ~50 km, calculated for an adiabatic geotherm, water-saturated olivine and a constant stress of 0.3 MPa, provides a minimum estimate for the viscosity in the mantle wedge of subduction zones. The upper bound on viscosity of the mantle wedge is calculated using a geotherm defined by the vapor-saturated solidus and a constant strain rate of 10^{-15}/s. The filled circle illustrates the viscosity of olivine aggregates calculated using estimates for pressure, temperature and water content derived from the composition of primitive arc magmas. The viscosity predicted for dry conditions at a constant temperature of 900°C illustrates the possible contrast in viscosity between the mantle wedge and the subducted slab.

conditions with an adiabatic geotherm. Because the temperature in the mantle wedge is likely always above the solidus, the viscosities could be somewhat lower if there is a significant amount of melt present. For example, based on the relationships in Figure 8, with a melt fraction of 2% the viscosity would be reduced by an additional factor of two. However, it is important to realize that the low viscosities shown in Figure 11 require both high temperatures and high water contents. Such a situation would necessitate a large flux of water into an adiabatically convecting mantle.

The temperature and water content of olivine in the mantle wedge can be constrained using petrologic data on arc lavas. For example, analyses of primitive andesites with ~6 wt% H_2O indicate equilibration with mantle peridotite at ~1200°C and 1.0 GPa [*Baker et al.,* 1994; *Gaetani and Grove,* this volume]. In Figure 12 we show the water content of olivine in equilibrium with water-saturated melt and basaltic melts with water contents of 2-6 wt%, using the distribution coefficients of *Hirth and Kohlstedt* [1996]. We previously hypothesized that the distribution coefficient for water between olivine and basaltic melt increases with increasing depth (pressure) because of differences in the solubility mechanism of water between the two phases (indicated by differences in the effect of water fugacity on water content). Recent measurements of these distribution coefficients are similar to those that we estimated using the solubility data [*Koga et al.,* 2002]. These relationships indicate that at a depth of ~30 km (pressure of 1 GPa), olivine in equilibrium with basalt with 6 wt% H_2O will contain 400-500 H/10^6Si. Using our dislocation creep flow law, we calculate a viscosity of 3×10^{19} Pas for olivine aggregates with a water content of 500 H/10^6Si, at a temperature of 1200°C, a pressure of 1.0 GPa and a differential stress of 0.3 MPa. This value is shown by the circle in Figure 11.

Numerical modeling studies also suggest that the viscosity of the mantle wedge is relatively low. *Billen and Gurnis* [2001] demonstrate that constraints on the geoid, gravity and topography above subuction zones are satisified if the viscosity of the mantle wedge is at least an order of magnitude less than that of the surrounding asthenosphere. Similar models suggest that the viscosity in the wedge may be as low as 4×10^{18} Pa s [Han, L., and Gurnis, M., Subduction in semi-dynamic models and application to the Tonga-Kermadec subduction zone, unpublished manuscript]. Based on the extrapolations of laboratory data shown in Figure 11, such a low viscosity requires both relatively high water contents and temperatures.

The contrast in viscosity between a subducted slab and the mantle wedge is difficult to quantify due to the nonlinear nature of rheology. For illustrative purposes, in Figure 11 we show the viscosity of a dry slab with a constant temperature of 900°C and a constant strain rate of $10^{-15}s^{-1}$. We use a dry rheology for the slab based on the hypothesis that water is removed from the oceanic lithosphere during melting at oceanic spreading ridges [e.g., *Hirth and Kohlstedt,* 1996]. Due to the strong temperature-dependence on viscosity, the colder interior regions of the slab would have an even greater viscosity than that predicted in Figure 11.

We reiterate that the magnitudes of viscosity shown in Figure 10 and Figure 11 are strongly dependent on the differential stress. The stress state in the wedge will be partly controlled by buoyancy resulting from temperature variations and the presence of melt. Ultimately, quantification of these effects will require analyses of dynamic models that couple the details of mantle rheology discussed in this paper with the dynamics of fluid migration into the wedge and the melting processes within the wedge.

Could the Subduction Factory Produce the oil of Plate Tectonics?

One of the requirements for Earth-like plate tectonics is that the boundaries of the plates must be considerably weak-

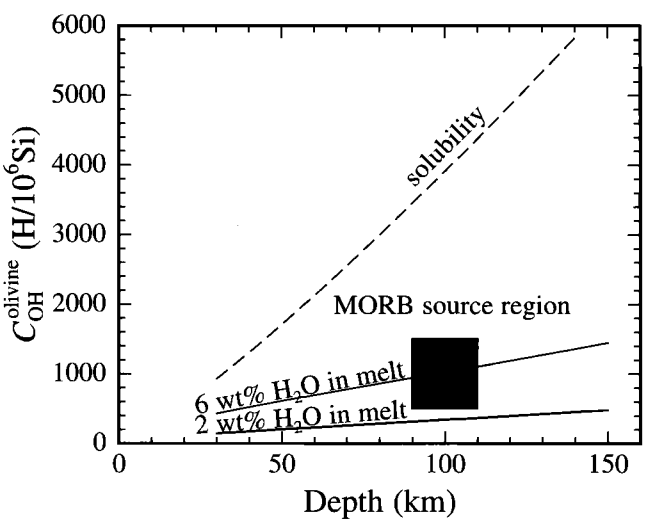

Figure 12. Plot of the water content of olivine in equilibrium with hydrous melt as a function of depth. The dashed line labeled solubility shows the water content of olivine under water-saturated conditions. The solid lines show the water content of olivine in equilibrium with basaltic melts with constant water contents of 2 wt.% and 6 wt.%. The shaded box shows the water content estimated for olivine in the oceanic asthenosphere. This plot suggests that the water content of olivine in the residue of arc magmatism is similar to that of olivine in the asthenosphere.

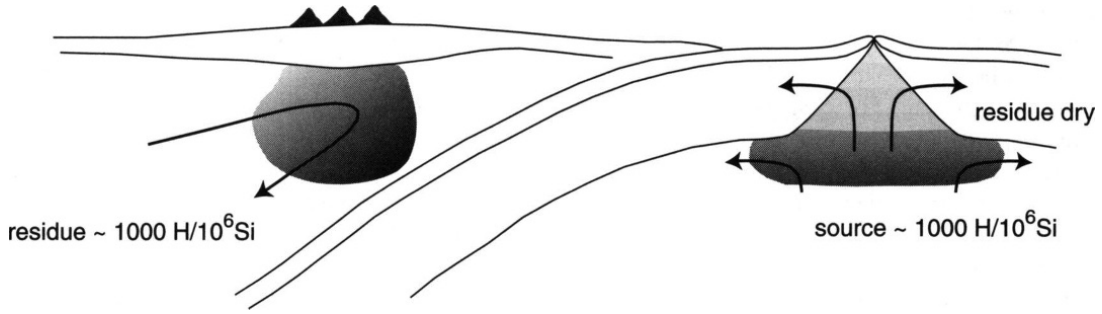

Figure 13. Cartoon illustrating fundamental differences in the role of water in the melting regions of arcs and ridges. At mid-ocean ridges, the melting process produces a dry residue. By contrast, the melting process at arcs produces a hydrous residue with a water content similar to that estimated for the oceanic asthenosphere, i.e., the MORB source region. Mantle flow lines are indicated by curved arrows. Shading indicates water content in the melting regions, with darker shades for higher water contents.

er than the plates. In addition to the plate boundaries defined by the subduction zones, the melting processes at arcs can influence tectonics by producing mantle with a water content similar to that of the asthenosphere. The relatively high water content of nominally anhydrous minerals in the oceanic mantle can create a rheological contrast between the asthenosphere and the overlying lithosphere. The viscosity of the lithosphere is increased relative to that of the asthenosphere partly because water is extracted from the residue during the melting process at oceanic ridges [*Hirth and Kohlstedt,* 1996; *Phipps Morgan,* 1997]. By contrast, due to the flux of fluids from the subducting slab into the mantle wedge, the melting process at subduction zones produces a relatively water-rich residue.

Another major difference between melting processes at ridges and subduction zones is that the residue of arc melting is advected downward by plate-driven flow. To explore the significance of this difference, we estimate the water content of olivine in the residue of arc melting. As shown in Figure 12, at a depth of ~100 km the water content of olivine in equilibrium with basaltic melt with a water content of 6 wt% is similar to that estimated for olivine in the MORB source [*Hirth and Kohlstedt,* 1996]. As illustrated in Figure 13, this observation suggests that the melting process in arcs may set the water content of nominally anhydrous phases in the asthenosphere. Thus transport of water from the slab into the mantle wedge can continually replenish the water content of the upper mantle and therefore facilitate the existence of a low viscosity asthenosphere.

Acknowledgments. We are grateful to the many colleagues with whom we have discussed the issues presented in this manuscript. In particular, we want to thank Shenghua Mei, Steve Mackwell, Mark Zimmerman, Peter Kelemen, Glenn Gaetani, Brian Evans, Magali Billen, Mike Braun, Laurent Montesi and Mathew Jull. We are also grateful for helpful reviews from Jed Mosenfelder and John Eiler. In addition, we want to thank Karen Hanghoj for assistance in preparing the manuscript. Finally, we would like to thank Sally Gregory Kohlstedt and Ann Mulligan for patience during several week long get-togethers where the authors hashed over endless details on olivine rheology. This work was supported by OCE-0099316 (GH), EAR-9910899 (GH), EAR-9906986 (DLK), OCE-0002463 (DLK), EAR-0126277 (DLK) and INT-0123224 (DLK).

REFERENCES

Ave Lallemant, H.G., J.-C., Mercier, N.L. Carter, and J.V. Ross, Rheology of the upper mantle: inferences from peridotite xenoliths, *Tectonophys.,* 70, 85-113, 1980.

Bai, Q., Mackwell, S.J., and Kohlstedt, D.L., High-temperature creep of olivine single crystals 1. Mechanical results for buffered samples. *J. Geophys. Res.,* 96, 2441-2463, 1991.

Bai, Q., and D.L. Kohlstedt, High-temperature creep of olivine single crystals; 2, Dislocation structures, *Tectonophysics,* 206, 1-29, 1992.

Bai, Q., Z. Jin, H.W. Green, Experimental investigation of partially molten peridote at upper mantle pressure and temperatue, in M. Holness (ed) *Deformation enhanced Fluid Transport in the Earth's Crust and Mantle,* Chapmann & Hall, 1997.

Baker, M.B., T.L. Grove, and R. Price, Primitive basalts and andesites from the Mt. Shasta region, N. California: products of varying melt fraction and water content, *Contrib. Mineral Petrol.,* 118, 111-129, 1994.

Beeman, M.L., and D.L. Kohlstedt, Deformation of olivine-melt aggregates at high temperatures and confining pressures, *J. Geophys. Res.,* 98, 6443-6452, 1993.

Bejina, F., P. Raterron, J. Zhang, O. Jaoul, and R. C. Lierbermann, Activation volume of silicon diffusion in San Carlos olivine, *Geophys. Res. Lett.,* 24, 25972600, 1997.

Bell, D.R., G.R. Rossman, A. Maldene, D. Endisch, and F. Rauch, Hydroxide in olivine: a quantitative determination of the

absolute amount and calibration of the IR spectrum, *J. Geophys. Res.*, in press, 2002.

Billen, M.I., and M. Gurnis, A low viscosity wedge in subduction zones, *Earth Planet. Sci. Lett.*, 193, 227-236, 2001.

Borch, R.S., and H.W. Green II, Deformation of peridotite at high pressure in a new molten salt cell: Comparison of traditional and homologous temperature treatments, *Phys. Earth Planet. Inter.*, 55, 269-276, 1989.

Braun, M. G. Hirth, and E.M. Parmentier, The effects of deep, damp melting on mantle flow and melt generation beneath mid-ocean ridges, *Earth Planet. Sci. Lett.*, 176, 339-356, 2000.

Chopra, P.N., and M.S. Paterson, The experimental deformation of dunite, *Tectonophys.*, 78, 453-473, 1981.

Chopra, P.N. and M.S. Paterson, The role of water in the deformation of dunite, *J. Geophys. Res.*, 89, 7861-7876, 1984.

Christensen, U.R., *Mantle rheology, constitution, and convection, in Mantle convection; plate tectonics and global dynamics,* Peltier, W. Richard (editor), 595-655, 1989.

Coble, R.L., A model for boundary diffusion controlled creep in polycrysatlline materials, *J. Appl. Phys.*, 34, 1679-1682, 1963.

Cooper, R.F., and D.L. Kohlstedt, Solution-precipitation enhanced diffusional creep of partially molten olivine basalt aggregates during hot-pressing, *Tectonophysics,* 107, 207-233, 1984.

Cooper, R.F., D.L. Kohlstedt, and K. Chyung, Solution-precipitation enhanced creep in solid-liquid aggregates which display a non-zero dihedral angle, *Acta Metall.*, 37, 1759-1771, 1989.

Craig, C.H., and D. McKenzie, The existence of a thin low-viscosity layer beneath the lithosphere, *Earth Planet. Sci. Lett.*, 78, 420-426, 1986.

Daines, M. J., and D. L. Kohlstedt, A laboratory study of melt migration, *Phil. Trans. R. Soc. Lond. A,* 342, 43-52, 1993.

de Bresser, J.H.P., J.H. ter Heege, and C.J. Spiers, Grain size reduction by dynamic recrystallization: can it result in major rheological weakening? *Int. J. Earth Sci. (Geologische Rundschau),* 90, 28-45, 2001.

Dohmen, R., S. Chakraborty, and H.-W. Becker, Si and O diffusion in olivine and implications for characterizing plastic flow in the mantle, submitted, 2002.

Durham, W.B., and C. Goetze, Plastic flow of oriented single crystals of olivine, 1, Mechanical data, *J. Geophys. Res.*, 82, 5737-5753, 1977.

Durham, W.B., L.A. Stern, and S.H. Kirby, Rheology of ice I at low stress and elevated confining pressure, *J. Geophys. Res.*, 106, 11,031-11,-42, 2001.

Evans, B., J. Fredrich, and T.-f Wong, The brittle-ductile transition in rocks; recent experimental and theoretical progress, in *The brittle-ductile transition in rocks,* (editors) Duba, A. G., W.B. Durham, J.W. Handin, and H.F. Wang, Geophysical Monograph, 56, 1-20, 1990.

Evans, B., J. Renner, and G. Hirth, A few remarks on the kinetics of grain growth in rocks, *Int. J. Earth Sci., (Geologishe Rundschau),* 90, 88-103, 2001.

Farver, J.R., and R.A. Yund, Silicon diffusion in forsterite aggregates; implications for diffusion accommodated creep, *Geophys. Res. Lett.*, 27, 2337-2340, 2000.

Fisler, D. K., and S.J. Mackwell, Kinetics of diffusion-controlled growth of fayalite, *Phys. Chem. Min.*, 21, 156-165, 1994.

Frost, H.J., and M.F. Ashby, *Deformation Mechanism Maps,* Pergamon Press, 1982.

Gaetani, G.A., and E.B. Watson, Open system behavior of olivine-hosted melt inclusions, *Earth Planet. Sci. Lett.*, 183, 27-41, 2000.

Gaetani, G.A., and T.L. Grove, Experimental constraints on melt generation in the mantle wedge, this issue.

Gaherty, J.B., and T.H. Jordan, Lehmann discontinuity as the base of an anisotropic layer beneath continents, Science, 268, 1468-1471, 1995.

Goetze, C., and D.L. Kohlstedt, Laboratory Study of dislocation climb and diffusion in olivine, *J. Geophys. Res.*, 78, 5961-5971, 1973.

Goldsby, D.L., and D.L. Kohlstedt, Superplastic deformation of ice: Experimental observations, J. Geophys. Res., 106, 11,017-11,030, 2001.

Gribb, T.T., R.F. Cooper, Low-frequency shear attenuation in polycrystalline olivine; grain boundary diffusion and the physical significance of the Andrade model for viscoelastic rheology, *J. Geophys. Res.*, 103, 27,267-27,279, 1998.

Gribb, T.T., R.F. Cooper, The effect of an equilibrated melt phase on the shear creep and attenuation behavior of polycrystalline olivine, *Geophys. Res. Lett.*, 27, 2341-2344, 2000.

Hager, B.H., Mantle viscosity: A comparison of models from post-glacial rebound and from the geoid, plate driving forces, and advected heat flux, in: *Glacial Isostasy, Sea level and Mantle Rheology,* R. Sabadini et al., eds., Kluwer Academic Publishers, Netherlands, pp. 493-513, 1991.

Hirth, G., and D.L. Kohlstedt, Experimental constraints on the dynamics of the partially molten upper mantle: Deformation in the diffusion creep regime, *J. Geophys. Res,* 100, 1981-2001, 1995a.

Hirth, G., and D.L. Kohlstedt, Experimental constraints on the dynamics of the partially molten upper mantle 2. Deformation in the dislocation creep regime, *J. Geophys. Res.*, 100, 15,441-15,449, 1995b.

Hirth, G., and D.L. Kohlstedt, Water in the oceanic upper mantle: implications for rheology, melt extraction and the evolution of the lithosphere, *Earth Planet. Sci. Lett.*, 144, 93-108, 1996.

Hirth, G., Evans, R.L., and A.D. Chave, Comparison of continental and oceanic mantle electrical conductivity: Is the Archean lithosphere dry?, *Geochemistry, Geophysics, and Geosystems (G^3)*, 1, Paper Number 2000CG000048, 2000.

Holtzman, B., M.E. Zimmerman, D.L. Kohlstedt, and J. Phipps Morgan, Interactions of deformation and fluid migration I: Melt segregation in the viscous regime, *Eos Trans. AGU,* 82(47), 2001

Houlier, B., M. Cheraghmakani, and O. Jaoul, Silicon diffusion in San Carlos Olivine, *Phys. Earth Planet. Int.*, 62, 329-340, 1990.

Jin, Z. M., Q. Bai, and D.L. Kohlstedt, High-temperature creep of olivine crystals from four localities, *Phys. Earth Planet. Int.*, 82, 55-64, 1994.

Karato, S.-I., Comment on 'The effect of pressure on the rate of dislocation recovery in olivine' by D.L. Kohlstedt, H.P.K. Nichols, and Paul Hornack, *J. Geophys. Res.,* 86, 9319, 1981.

Karato, S., and M. Ogawa, High-pressure recovery of olivine; implications for creep mechanisms and creep activation volume, *Phys. Earth Planet. Int.,* 28, 102-117, 1982.

Karato, S., Grain-size distribution and rheology of the upper mantle, *Tectonophys.,* 104, 155-176, 1984.

Karato, S., M.S. Paterson and J.D. FitzGerald, Rheology of synthetic olivine aggregates: influence of grain size and water, J. Geophys. Res. 91, 8151-8176, 1986.

Karato, S., On the Lehmann Discontinuity, *Geophys. Res. Lett.,* 19, 2255-2258, 1992.

Karato, S., Wu, P., Rheology of the upper mantle; a synthesis, *Science,* 260, 771-778, 1993.

Karato, S., D.C., Rubie, and H. Yan, Dislocation recovery in olivine under deep upper mantle conditions; implications for creep and diffusion, *J. Geophys. Res.,* 98, 9761-9768, 1993.

Karato, S., and D.C. Rubie, Toward an experimental study of deep mantle rheology; a new multianvil sample assembly for deformation studies under high pressures and temperatures, *J. Geophys. Res.,* 102, 20,111-20, 1997.

Karato, S., Mapping water content in the upper mantle, this issue.

Karato, S., and H. Jung, Effects of pressure on high-temperature dislocation creep in olivine, in press, *Philosophical Magazine A.,* 2002.

Kelemen, P.B., G. Hirth, N. Shimizu, M. Spiegelman and H.J.B. Dick, A review of melt migration processes in the adiabatically upwelling mantle beneath spreading ridges, *Philos. Trans. R. Soc. London A,* 355, 283-318, 1997.

Kelemen, P.B., J.L. Rilling, E.M. Parmentier, L. Mehl, and B.R. Hacker, Thermal structure due to solid-state flow in the mantle wedge beneath arcs, [this issue]

Keyes, R.W., Continuum models of the effect of pressure on activated processes, *in Solids Under Pressure,* edited by W. Paul and D. M. Warschauer, 71-99, McGraw-Hill, New York, 1963.

Koga, K, E. Hauri, M. Hirshmann, and D. Bell, Hydrogen concentration analyses using SIMS and FTIR: Comparsion and calibration for nominally anhydrous minerals, *G-cubed,* in press, 2002.

Kohlstedt, D.L., and C. Goetze, Low-stress high-temperature creep in olivine single crystals, *J. Geophys. Res.,* 79, 2045-2051, 1974.

Kohlstedt, D. L., H.P.K. Nichols, and P. Hornack, P., The effect of pressure on the rate of dislocation recovery in olivine, *J. Geophys. Res.,* 85, 3122-3130, 1980.

Kohlstedt, D.L., H. Keppler and D.C. Rubie, Solubility of water in a, b, and g phases of $(Mg,Fe)_2SiO_4$, *Contrib. Min. Pet.,* 123, 345-357, 1996.

Kohlstedt, D. L., and M. E. Zimmerman, Rheology of partially molten mantle rocks, *Ann. Rev. Earth Planet. Sci.,* 24, 41-62, 1996.

Kohlstedt, D.L., and S.J. Mackwell, Diffusion of hydrogen and itrinsic point defects in olivine, *Z. Phys. Chem.,* 207, 147-162, 1998.

Kohlstedt, D.L., Q. Bai, Z.-C. Wang, and S. Mei, Rheology of partially molten rocks, in *Physics and Chemistry of Partially Molten Rocks,* ed. N.Bagdassarov, D. Laporte, A.B.Thompson, Kluwer Academic Publishers, 3-28, 2000.

Kohlstedt, D.L. and Wang, Z., Grain-Boundary Sliding Accommodated Dislocation Creep in Dunite, *Eos Trans. AGU,* 82(47), 2001.

Kumazawa, M., and O. Anderson, Elastic moduli, pressure derivatives, and temperature derivatives of single-crystal olivine and single-crystal forsterite, *J. Geophys. Res.,* 74, 5961-5972, 1994.

Langdon, T.G., A unified approach to grain boundary sliding in creep and superplasticity, *Acta Metall.,* 42, 2437-2443, 1994.

Mackwell, S.J., K.L. Kohlstedt, M.S. Paterson, The role of water in the deformation of olivine single crystals, *J. Geophys. Res.,* 90, 11319-11333, 1985.

Mackwell, S.J., G. Hirth, and D.L. Kohlstedt, Water weakening of olivine single crystals, *Deformation mechanisms in nature and experiment, Conference,* Basel, Switzerland, 1997.

Mei, S., and D.L. Kohlstedt, Influence of water on deformation of olivine aggregates; 1, Diffusion creep regime, *J. Geophys. Res.,* 105, 21,457-21,469, 2000a

Mei, S., and D.L. Kohlstedt, Influence of water on plastic deformation of olivine aggregates 2. Dislocation creep regime, J. Geophys. Res., 105, 21471-21481, 2000b.

Mei, S., W. Bai, T. Hiraga, and D.L. Kohlstedt, Ifluence of melt on plastic deformation of olivine-basalt aggregates under hydrous conditions, *Earth Planet. Sci. Lett.,* in press, 2002.

Melosh, H.J., Nonlinear stress propagation in the Earth's upper mantle, J. Geophys. Res., 81, 5621-5632, 1976

Nicolas, A., Structure and petrology of peridotites: clues to their geodynamic environment, *Rev. Geophys.,* 24, 875-895, 1986.

Ohtani, E. , and M. Kumazawa, Melting of forsterite Mg2SiO4 up to 15 GPa, Phys. *Earth Planet. Int.* 27, 32-38, 1981.

Panasyuk, S.V., and B.H. Hager, Inversion for mantle viscosity profiles constrained by dynamic topography and the geoid, and their estimated errors, *Geophys. J. Int.,* 143, 821-836, 2000.

Paterson, M.S., The ductility of rocks, in *Physics of Strength and Plasticity,* edited by A.S. Argon, 377-392, MIT Press, Cambridge, Mass., 1969.

Paterson, M.S., The determination of hydroxyl by infrared absorption in quartz silicate glasses and similar materials, *Bull. Mineral.,* 105, 20-29, 1982.

Peltier, W.R., Global glacial isostasy and relative sea level: Implications for solid earth geophysics and climate system dynamics, in *Dynamics of the Ice Age Earth,* P. Wu (editor), 17-54, 1998.

Phipps Morgan, J. The generation of a compositional lithosphere by mid-ocean ridge melting and its effect on subsequent off-axis hot spot upwelling and melting, Earth Planet Sci. Lett., 146, 213-232, 1997.

Poirier, J.-P., *Creep of Crystals,* Cambridge University Press, 1985.

Raj, R., and M.F. Ashby, On grain boundary sliding and diffusional creep, *Metall. Trans.,* 2, 1113-1127, 1971.

Renner, J., B. Evans, and G. Hirth, On the rheologically critical melt percentage, *Earth Planet. Sci. Lett.,* 181, 585-594, 2000.

Renner, J., K.Viskupic, G. Hirth, and B. Evans, Melt extraction

from partially molten peridotites, submitted, *Geochemistry, Geophysics, and Geosystems (G^3)*, in press, 2002.

Ricoult, D. L., and D.L. Kohlstedt, Experimental evidence for the effect of chemical environment upon the creep rate of olivine, in *Point defects in minerals,* Schock, R.N. (editor) Geophysical Monograph, 31, 171-184, 1985.

Ross, J. V., H.G. Ave Lallemant, and N.L. Carter, Activation volume for creep in the upper mantle, *Science,* 203, 261-263, 1979.

Ryerson, F. J., W.B. Durham, D.J., Cherniak, and W.A. Lanford, Oxygen diffusion in olivine; effect of oxygen fugacity and implications for creep, *J. Geophys. Res.,* 94, 4105-4118, 1989.

Sammis, C.G., J.C. Smith and G. Shubert, A critical assessment of estimation methods for activation volume, *J. Geophys. Res.,* 86, 10,707-10,718, 1981.

Schwenn, M. B., and C. Goetze, Creep of olivine during hot-pressing, *Tectonophysics,* 48, 41-60, 1978.

Tommasi, A., D. Mainprice, G. Canova, and Y. Chastel, Viscoplastic self-consistent and equilibrium-based modeling of olivine preferred orientations: Implications for the upper mantle seismic anisotropy, *J. Geophys., Res.,* 105, 7893-7908, 2000.

Toomey, D. R. W.S.D. Wilcock, J.A. Conder, D.W. Forsyth, J.D. Blundy, E.M. Parmentier, and W.C. Hammond, Asymmetric mantle dynamics in the MELT region of the East Pacific Rise, *Earth Planet. Sci. Lett.,* 200, 287-295, 2002.

Toramaru, A., and N. Fujii, Connectivity of melt phase in a partially molten peridotite, J. *Geophys. Res.,* 91 9239-9252, 1986.

Watson, E. B., Diffusion in fluid-bearing and slightly melted rocks; experimental and numerical approaches illustrated by iron transport in dunite, *Cont. Min. Petrol.,* 107, 417-434, 1991.

Weertman, J., The creep strength of the Earth's mantle, *Rev. Geophys. Space Phys.* 8, 145-168, 1970.

Xu, Y., M.E. Zimmerman, and D.L.Kohlstedt, Deformation behavior of partially molten mantle rocks, *MARGINS Theoretical and Experimental Earth Science Series. Volume I: Rheology and Deformation of the Lithosphere at Continental Margins,* eds. G.D. Karner, N.W. Driscoll, B. Taylor and D.L. Kohlstedt, Columbia University Press, in press, (2002).

Young, T.E., H.W. Green II, A.M. Hofmeister and D. Wallker, Infrared spectroscopic investigation of hydroxyl in β-$(Mg,Fe)_2SiO_4$ and coexisting olivine: Implications for mantle evolution and dynamics, *Phys. Chem. Miner.,* 19, 409-422, 1993.

Zener, C., Theory of lattice expansion introduced by cold-work, *Trans. AIME,* 147, 361-368, 1942.

Zhang, S., S.-I. Karato, J. FitzGerald, U.H. Faul, and Y. Zhou, Simple shear deformation of olivine aggregates, *Tectonophysics,* 316, 133-152, 2000.

Zhang, J., and C. Herzberg, Melting experiments on anhydrous peridotite KLB-1 from 5.0 to 22.5 GPa, *J. Geophys. Res.,* 99, 17,729-17,742, 1994.

Zimmerman, M.E., *The Structure and Rheology of Partially Molten Mantle Rocks,* Ph.D. Thesis University of Minnesota, 159 pp., 1999

Greg Hirth, Department of Geology and Geophysics, Woods Hole Oceanographic Institution, Woods Hole, MA 02543. (ghirth@whoi.edu)

D.L. Kohlstedt, Department of Geology and Geophysics, University of Minnesota-Twin Cities, Pillsbury Hall, Minneapolis, MN 55455. (dlkohl@umn.edu)